Formation of a Carbinolamine Intermediate in the Tertiary Amine Catalyzed Enolization of Oxaloacetic Acid. An Alternative Mechanism for Enolization[1,2]

Paula Yurkanis Bruice

Contribution from the Department of Chemistry, University of California, Santa Barbara, California 93106. *Received November 15, 1982*

Abstract: The keto–enol and keto–hydrate equilibria of oxaloacetic acid have been investigated in aqueous solution in the presence of lyate species and in the presence of both oxygen base catalysts and tertiary amine catalysts. Lyate species and oxygen bases catalyze the interconversion of keto–enol tautomers by the well accepted acid and base catalyzed mechanisms of eq 1 and 2; Brønsted $\beta = 0.32$, $\alpha = -0.43$. The second-order rate constants for catalysis by tertiary amines are from 800 to 2200 (depending on the pK_a of the tertiary amine) times greater than the oxygen base second-order rate constants, a rate acceleration too great to be attributed to the enhanced ability of tertiary amines in proton removal. The tertiary amine buffer dilution plots exhibit a nonlinear dependence of rate on amine concentration at low tertiary amine concentrations. The intercepts at zero amine concentration of the linear portions of the tertiary amine buffer dilution plots are more than 100-fold greater than can be attributed to lyate species catalyzed keto–enol interconversion and more than 10-fold greater than can be attributed to lyate species catalyzed keto–hydrate interconversion, suggesting that in the tertiary amine catalyzed enolization reaction lyate species is operating not on keto, enol, or hydrate but on some reactive intermediate. In order to account for these observations, the tertiary amine catalyzed interconversion of keto–enol tautomers is proposed to occur through the mechanism of eq 3, which involves the formation of a carbinolamine intermediate followed by amine catalyzed elimination of a proton and tertiary amine. The β value for reaction of tertiary amines with oxaloacetic acid is 0.24. Severely sterically hindered tertiary amines do not follow the nucleophilic addition–elimination mechanism of eq 3 but, like oxygen bases, catalyze enolization via the general base catalyzed mechanism of eq 2. Enolate protonation rates were also determined; Brønsted $\alpha = -0.59$ for oxygen acids and -0.78 for protonated tertiary amines.

Introduction

The mechanism of the interconversion of keto–enol tautomers was one of the first organic reaction mechanisms to be studied, and it has subsequently received a great deal of attention.[3,4] It is well-known that tautomerization occurs via either an acid catalyzed mechanism (eq 1) or a base catalyzed mechanism (eq

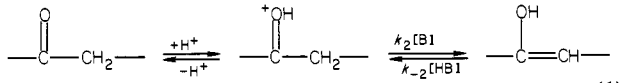

(1)

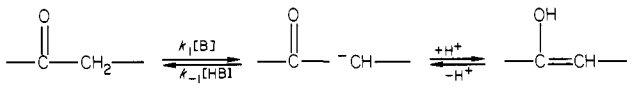

(2)

2). Both mechanisms involve rate-limiting removal of a proton from the α-carbon atom in the forward direction and rate-limiting donation of a proton to the α-carbon atom in the reverse direction. We previously reported that when the basic catalyst is a tertiary amine, the enolization of oxaloacetic acid occurs by a more facile mechanism than the base catalyzed mechanism of eq 2, which takes place in the presence of oxygen bases.[5] The tertiary amine, rather than initially removing a proton from the α-carbon atom of the ketone, attacks the carbonyl carbon atom to form a carbinolamine intermediate (eq 3). A second molecule of tertiary amine then catalyzes the elimination of a proton and neutral amine from the carbinolamine to give enol.

Emly and Leussing subsequently reported that there was no need to invoke a mechanism other than that shown in eq 2 for the tertiary amine catalyzed enolization of oxaloacetic acid.[6] They argued that the evidence we obtained to support the mechanism

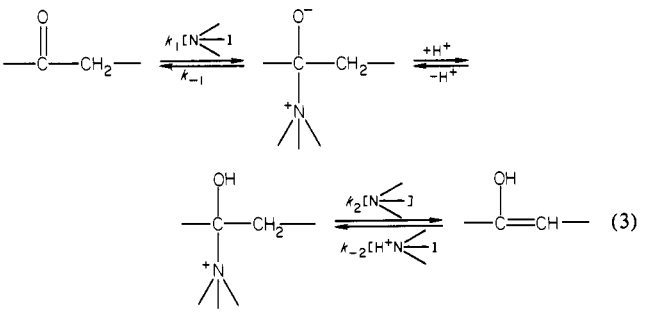

(3)

of eq 3 could be attributed to our measuring the perturbation of the keto–hydrate equilibrium rather than the keto–enol equilibrium of oxaloacetic acid.

Since it is of importance to a variety of organic reaction mechanisms to ascertain whether a tertiary amine can act to increase the lability of an atom or group of atoms attached to a carbon α to a carbonyl group, we have reinvestigated the tertiary amine catalyzed enolization of oxaloacetic acid. We have examined the reaction of nine tertiary amines, ranging in pK_a from 6.2 to 11.2, with oxaloacetic acid under conditions where their catalytic effect on both keto–enol and on keto–hydrate interconversion could be monitored. We now offer evidence that eight of the nine tertiary amines catalyze keto–enol tautomerization via the mechanism of eq 3. The evidence for the occurrence of this mechanism is based on the following observations: (a) there exists a nonlinear dependence of rate on amine concentration at low amine concentration; (b) the second-order rate constants for catalysis of keto–enol interconversion by tertiary amines are more than 1000-fold greater than those for catalysis by oxygen bases of the same pK_a; (c) at high amine concentration, where a linear dependence of rate on amine concentration is observed, extrapolation to zero amine concentration gives a rate for the lyate species catalyzed reaction that is more than 500-fold greater than can be attributed to lyate species catalysis of the enolization mechanisms of eq 1 and 2 and more than 10-fold greater than can be attributed to lyate species catalysis of keto–hydrate interconversion. One of the tertiary amines we examined was found to catalyze keto–enol interconversion via the mechanism of eq 2. This was 2-(diisopropylamino)ethanol whose considerable steric bulk pre-

(1) This work was supported by a grant to T. C. Bruice from the National Institutes of Health.
(2) The author expresses her gratitude to Huey-Ching Su and Ronald W. Raab for their superb technical assistance and dedication.
(3) Bell, R. P. "Acid-Base Catalysis"; Oxford University Press: London, 1941.
(4) Bell, R. P. "The Proton in Chemistry"; Cornell University Press: Ithaca, NY, 1973.
(5) Bruice, P. Y.; Bruice, T. C. *J. Am. Chem. Soc.* **1978**, *100*, 4793.
(6) (a) Emly, M.; Leussing, D. L. *J. Am. Chem. Soc.* **1981**, *103*, 628. (b) Emly, M. Ph.D. Thesis, The Ohio State University, Columbus, OH, 1979.

0002-7863/83/1505-4982$01.50/0

vents it from participating in the nucleophilic addition–elimination mechanism of eq 3.

Experimental Section

Materials. Oxaloacetic acid (Aldrich) was recrystallized twice from a 50/50 mixture of acetone and benzene. Anal. Calcd for $C_4H_4O_5$: C, 36.38; H, 3.05. Found: C, 36.19; H, 3.09. Other reagents have been described previously.[5]

Buffer Solutions. The amine–amine hydrochloride buffer solutions were prepared immediately prior to use by the addition of standardized KOH or HCl to the amine hydrochloride or free amine. Carbonate buffer solutions were prepared by using K_2CO_3 and 1.0 M HCl; for phosphate buffers, KH_2PO_4 and 1.0 M KOH were used. All buffer solutions were maintained at μ = 0.5 (KCl) and contained 1×10^{-4} M EDTA. The pHs of the serially diluted buffer solutions were adjusted when necessary so that the pH of the effluent from the stopped-flow spectrophotometer agreed within ±0.03 pH units for each of the serial dilutions. The pK_as of the buffers employed were determined by half-neutralization at 30 °C and μ = 0.5. Readings of pH were determined on a Radiometer Type 26 pH meter.

Kinetic Measurements. All kinetic determinations were carried out in doubly glass-distilled water containing 10^{-4} M EDTA to sequester extraneous metal ions, with μ = 0.5 (KCl). Occasional kinetic determinations were carried out in solutions containing 10^{-3} M EDTA and in the absence of EDTA to confirm that EDTA had no effect on any of the rate processes observed. All rate constants were determined at 30.0 ± 0.2 °C.

The rates of keto–enol interconversion shown in the pH-rate profile of Figure 2 (solid line) between pH 5 and 10 were obtained by using a Radiometer pH-stat assembly specifically designed for a Cary 15 spectrophotometer.[7] All other rate constants, including all rate constants determined in the presence of oxygen base buffers and amine buffers, were determined by using a Durrum D-150 or D-110 stopped-flow spectrophotometer equipped with a Biomation Model 805 waveform recorder. To minimize pH changes upon mixing, uneven (1:5) mixing cylinders were used; the smaller cylinder was used for the oxaloacetate solution and the larger cylinder for the buffer solution. Each experiment was carried out with a freshly prepared solution of oxaloacetate (in 0.5 M KCl containing 10^{-4} M EDTA). The pH of the oxaloacetate solution was adjusted to either 2.2 or 12.3; thus, when mixed with buffer (pH 5.2–11.5), the reactions occurring after either a rapid increase or a rapid decrease in pH could both be monitored. When buffer solutions were employed, the reactions were carried out under the pseudo-first-order conditions of $[\text{buffer}]_T \gg [\text{oxaloacetate}]$. After mixing, the final concentration of oxaloacetate in the kinetic solution was 6.0×10^{-5} M. All spectrophotometers were thermostated. Rates were determined by following the change in absorbance at 270 nm except when the reaction was buffered with 3-chloroquinuclidine, in which case the reactions were monitored at 290 nm because of buffer absorbance at the shorter wavelength. The relative volumes of the mixing cylinders and the dead time of the spectrophotometers were checked by mixing 0.01 M $Fe(NO_3)_3$ in 0.1 N H_2SO_4 (large cylinder) and 0.05 M KSCN (small cylinder) solutions; the dead time was found to be less than 4 ms.

Calculation of rate constants was done with (a) the stopped-flow spectrophotometer interfaced to a North-Star microcomputer for data digitation and storage employing an On-Line Instrument Systems 3820 stopped-flow program with the capability of calculating both monophasic and biphasic rate processes,[8] and (b) manual digitation of rate traces using a Hewlett-Packard 9820A computer/9864A digitizer. Both methods of calculation resulted in essentially identical rate constants. When the biphasic rate processes were sufficiently separated in time, calculation treating them as two successive monophasic rates using two time constants for collection and storage of data was preferable to attempting to collect sufficient data for both rates using a single time constant. When both methods of calculation were used for biphasic rate processes, the rate constants obtained were in good agreement. All observed rate constants are the mean of at least three determinations. Calculation of least-square slopes and intercepts and generation of the theoretical pH–rate profiles were done with the HP 9820A computer.

Results

Composition of Oxaloacetic Acid. The reported distribution of ketone, hydrate, and enol in aqueous solutions of oxaloacetic acid as a function of pH is shown in Table I. Hydrate is most prevalent at pH values where both carboxyl groups of oxaloacetic acid are protonated (for the keto tautomer pK_{a1} = 2.22 and pK_{a2} = 3.98; for the enol tautomer pK_{a1} = 1.89 and pK_{a2} = 3.72).[10] A plot of the equilibrium absorbance at 270 nm of an aqueous solution of oxaloacetate as a function of pH in the absence and presence of tertiary amine is shown in Figure 1. Only enol and enolate anion absorb light at this wavelength; neither ketone nor hydrate evidence any significant absorbance. The increase in absorbance at low pH is due to increasing concentration of the enol tautomer as the hydrate–ketone equilibrium is shifted toward ketone upon ionization of the carboxyl groups (eq 4). Loss of

$$\text{hydrate} \rightleftarrows \text{ketone} \rightleftarrows \text{enol} \underset{+H^+}{\overset{-H^+}{\rightleftharpoons}} \text{enolate} \qquad (4)$$

a proton from the enol tautomer is responsible for the large increase in absorbance in the basic pH region. The absorbance plotted in Figure 1 can be expressed as in eq 5, where P is the

$$\text{OD} = P + \epsilon_{E^-} K_a/(K_a + a_H) \qquad (5)$$

absorbance due to hydrate, ketone, and enol, ϵ_{E^-} is the molar absorbtivity of enolate anion, and K_a is the third overall dissociation constant of oxaloacetic acid.[11] Rearrangement of eq 5 gives eq 6. A plot of $1/(\text{OD} - \text{P})$ vs. a_H, using the data of Figure 1 from

$$1/(\text{OD} - P) = 1/\epsilon_{E^-} + a_H/(\epsilon_E K_a) \qquad (6)$$

pH 11.5 to 12.5 and assuming P to remain constant in this pH range, results in a pK_a of 13.04 for the enol tautomer (inset to Figure 1). This is in agreement with the previously reported values of 13.01 and 13.03 for the third overall dissociation constant of oxaloacetic acid.[10,11]

Table I. Reported Composition of Aqueous Solutions of Oxaloacetic Acid as a Function of pH at 25 °C

pH	ketone, %	enol, %	hydrate, %	[E]/[K]	[H]/[K]
0.0	small	5	95		
1.0	8	7	85	0.88	10.6
1.3[a]	13	6	81	0.46	6.23
3.1	55	10	35	0.18	0.64
3.7	65	10	25	0.15	0.38
4.7	76	11	13	0.14	0.17
6.7[a]	87	7	6	0.08	0.07
6.9	81	12	7	0.15	0.09
12.7	73	21[b]	6	0.29	0.08

[a] Reference 9; all other values from ref 6. [b] Enol + enolate.

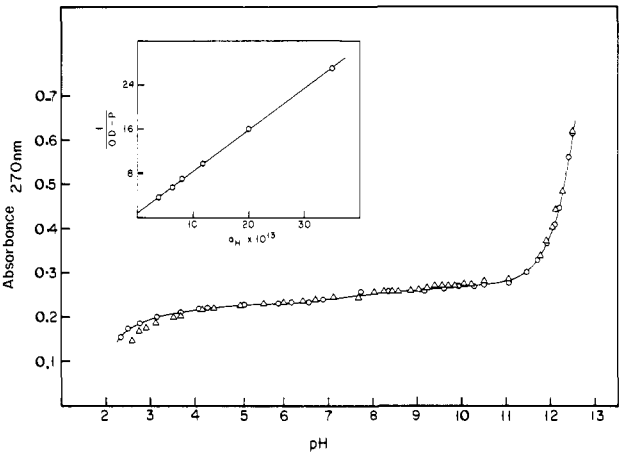

Figure 1. Absorbance at 270 nm of an equilibrated solution of oxaloacetic acid (1.13×10^{-4} M, μ = 0.5 (KCl), 30 °C) as a function of pH in (○) 0.5 M KCl and (△) 0.1 M trimethylamine minus the absorption of 0.1 M trimethylamine. Inset: Plot of $1/(\text{OD} - P)$ vs. a_H for determination of the pK_a of enolic oxaloacetic acid (eq 6).

(7) Maley, J. R.; Bruice, T. C. *Anal. Biochem.* **1970**, *34*, 275.
(8) On-Line Instrument Systems, Route 2, Jefferson, GA 30549.
(9) Kokesch, F. C. *J. Org. Chem.* **1976**, *41*, 3593.
(10) Tate, S. S.; Grzybowski, A. K.; Datta, S. P. *J. Chem. Soc.* **1964**, 1372.
(11) Bamann, E.; Sethi, V. S.; Laskavy, G. *Arch. Pharm. (Weinheim, Ger.)* **1968**, *301*, 12.

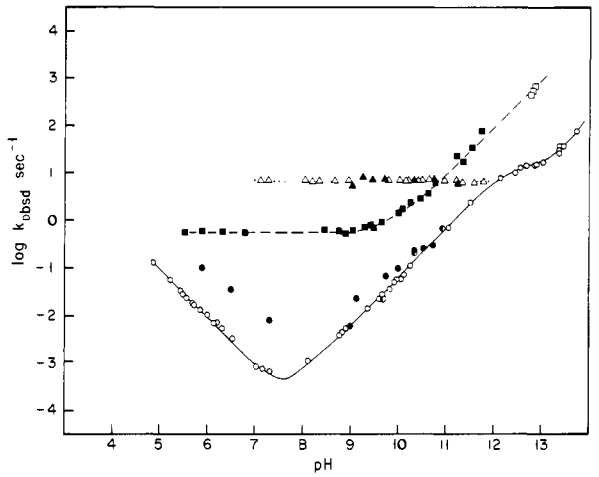

Figure 2. All rates determined in aqueous solution at 30 °C with μ = 0.5. Solid line: pH–rate profile for keto–enol interconversion of oxaloacetic acid. Rates determined in the presence of lyate species (○) and rates determined from intercepts of bufer dilution plots at zero buffer concentration employing carbonate and phosphate (●) and 2-(diisopropylamino)ethanol (◐) as buffers. Dashed line: pH–rate profile for keto–hydrate interconversion of oxaloacetic acid. Rates determined in the presence of lyate species (□) and rates determined from the intercepts of buffer dilution plots (k_{2N}) at zero buffer concentration employing tertiary amines as buffers (■). Dotted line: pH–rate profile for protonation of the enolate anion of oxaloacetic acid. Rates determined in the presence of lyate species (△) and rates determined from the intercepts of buffer dilution plots at zero buffer concentration employing carbonate and phosphate (▲) as buffers.

Catalysis by Lyate Species. For an explanation of the assignment of the observed rate processes to keto–enol or keto–hydrate interconversion based on the initial distribution of keto, enol, and hydrate and the observed absorbance changes, see Composition of Oxaloacetic Acid in the Discussion. The pH–rate profile for catalysis of keto–enol interconversion by lyate species (H_3O^+, H_2O, and HO^-) is given by the solid line of Figure 2. The rate constants (open circles) through which the solid line is drawn were determined by (a) mixing an oxaloacetate solution equilibrated at pH 2.2 with a more basic solution and monitoring the increase in absorbance due to overall enol formation occurring as a result of the sudden increase in pH (hereafter referred to as a pH increase experiment), and (b) mixing an oxaloacetate solution equilibrated at pH 12.3 with a more acidic solution and monitoring the decrease in absorbance occurring as the keto–enol equilibrium is shifted toward ketone as a result of the sudden decrease in pH (hereafter referred to as a pH decrease experiment). Rate constants, sufficiently small to be measured without employing stopped-flow techniques, were also obtained by using an ethanolic stock solution of enolic oxaloacetate and monitoring the decrease in absorption that occurs as the keto tautomer is formed in aqueous solution. At a given pH, the three procedures give rise to identical observed rate constants. The solid line of Figure 2, which is drawn through the experimental points, was computer generated from the following empirical equation:

$$k_{obsd} = k_H a_H + k_b K_a/(K_a + a_H) + k_{HO^-} K_w/a_H \quad (7)$$

where $k_H = 9.43 \times 10^3$ M^{-1} s^{-1}, $k_b = 11.4$ s^{-1}, $k_{HO^-} = 73.5$ M^{-1} s^{-1}, pK_a = 12.33, pK_w = 13.83, and a_H is the hydrogen ion activity determined at the glass electrode. The apparent pK_a of 12.33 obtained for the enol tautomer from eq 7 may be compared to the third overall titrimetric pK_a of 13.04 determined from Figure 1. The individual third dissociation constant of enolic oxaloacetate is equal to $K_a(1 + K_T)$, where K_a is the third overall dissociation constant and K_T is the tautomeric equilibrium constant ([K^{-2}]/[E^{-2}]). Tate et al. have reported a pK_a of 13.01 for the third overall dissociation constant and a pK_a of 12.18 for the individual dissociation constant of the enol tautomer.[10]

To ascertain that none of the rate processes determined in this study was due to reaction of substrate decomposition products, an investigation was made of the stability of oxaloacetic acid solutions at pH 12.3 and 2.2, the acidities at which the substrate solutions are initially equilibrated. At pH 12.3 decomposition of substrate takes place with a first-order rate constant of 3.4×10^{-5} s^{-1}, too slow for product decomposition to be a factor in this study. In addition, identical rate constants were obtained by using an oxaloacetic acid solution equilibrated at pH 2.2 and an oxaloacetic acid solution that had sat at pH 12.3 for 30 min before being adjusted to pH 2.2. At pH 2.2 there is no appreciable loss of enol absorbance over a 24-h period. However, because of the low concentration of enol present in acidic solutions, decomposition of substrate is difficult to monitor spectrally. The rate of decarboxylation of oxaloacetic acid has been determined enzymatically as a function of pH, and at pH 2.2 decarboxylation occurs with a rate constant of 1.8×10^{-5} s^{-1}.[11]

The pH–rate profile for water and hydroxide ion catalysis of keto–hydrate interconversion is given by the dashed line of Figure 2. Since neither ketone nor hydrate absorb at 270 nm and since lyate species catalyzed keto–hydrate interconversion is more rapid than lyate species catalyzed keto–enol interconversion, hydration rates could not be measured directly except in very basic solutions. The open squares on the dashed line represent rate constants obtained by mixing oxaloacetate equilibrated at pH 13.6 with a less basic solution to give the final pH indicated in Figure 2. The resulting pH change causes only a very small change in absorbance. Thus, for the reaction to be observable, the oxaloacetate concentration must be about 4 times greater than that normally employed. In the presence of tertiary amines (where the total concentration of tertiary amine is greater than ~0.02 M), keto–enol interconversion is faster than keto–hydrate interconversion. Under such circumstances, the rate of keto–hydrate interconversion can be monitored by the change in enol absorbance that occurs as the keto–enol equilibrium shifts to accommodate the slower, and consequently rate limiting, change in the keto–hydrate equilibrium (eq 4). The solid squares on the dashed line of Figure 2 represent the intercepts at zero amine concentration of buffer dilution plots of tertiary amine catalyzed keto–hydrate interconversion. The dashed line of Figure 2 was generated from eq 8, where $k_0 = 5.67 \times 10^{-1}$ s^{-1}, $k'_{HO^-} = 6.19 \times 10^3$ M^{-1} s^{-1}, and pK_w = 13.83.

$$k_{obsd} = k_0 + k'_{HO^-} K_w/a_H \quad (8)$$

The dotted line of Figure 2 is drawn through rate constants observed ($k_{obsd} = 6.70$ s^{-1}) when oxaloacetic acid equilibrated at pH 12.3 is mixed with more acidic solutions. The open triangles represent rate constants observed in the presence of lyate species; the solid triangles represent the intercepts at zero buffer concentration of general acid catalyzed buffer dilution plots (see below). This rate process is characterized by decreasing absorbance at 270 nm and is observed prior to the decrease in absorbance associated with keto–enol interconversion. This reaction is observed only in the pH decrease experiments; it is not observed when oxaloacetic acid is initially equilibrated at pH 2.2 and is subsequently made more basic. Presumably this initial rapid reaction may be attributed to protonation of enolate anion by water. The observed rate constant of 6.70 s^{-1} can be compared to the rate constant of 11.4 s^{-1} obtained for protonation of enolate anion by water in keto–enol interconversion (k_b of eq 7). The value of 11.4 s^{-1} was determined by the best fit of the solid line of Figure 2 to the experimental points and is dependent on an apparent pK_a of 12.33 for the enol tautomer; a value of 6.70 s^{-1} for k_b would require a slightly smaller pK_a of 12.10. Thus it is reasonable to assume that the kinetically apparent rate constant of 11.4 s^{-1} and the observed rate constant of 6.70 s^{-1} pertain to the same event. Brouillard and Dubois reported rate constants ranging from 1.3 to 8.0 s^{-1} for water protonation of a series of α-substituted ethyl acetoacetates.[12]

Catalysis by Oxygen Bases. The enolization of oxaloacetic acid was examined using oxygen bases as catalysts. The buffer dilution plots obtained with phosphate (HPO_4^{2-}/PO_4^{3-}) buffer evidence

(12) Brouillard, R.; Dubois, J. E. *J. Org. Chem.* **1974**, *39*, 1137.

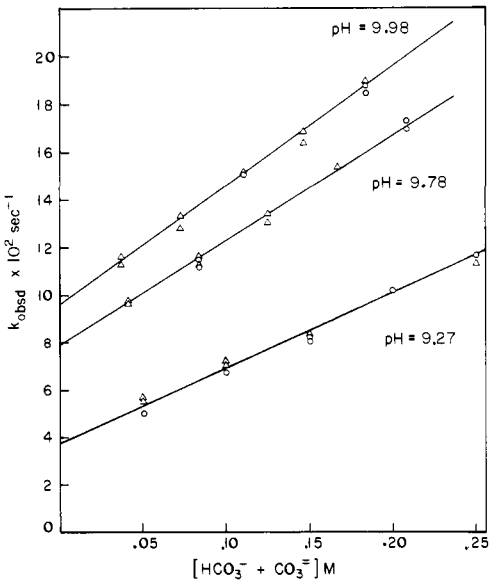

Figure 3. Plots of the observed first-order rate constants for the enolization of oxaloacetic acid in the presence of carbonate buffer vs. the total concentration of carbonate buffer at three hydrogen ion concentrations: (O) rate constants obtained from pH increase experiments; (Δ) rate constants obtained from pH decrease experiments.

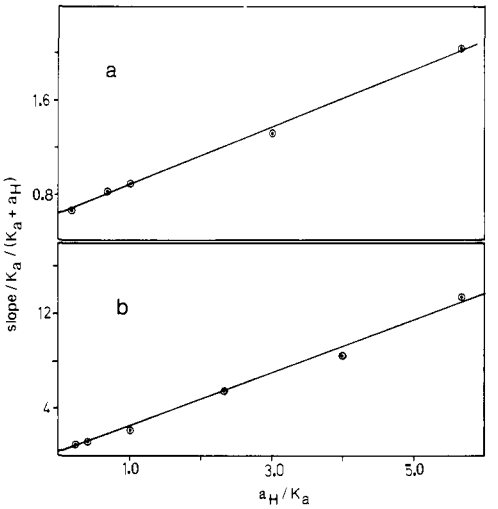

Figure 4. Plots of the slopes of buffer dilution plots divided by the mole fraction of buffer present in the basic form vs. the mole fraction of buffer present in the acidic form divided by the mole fraction of buffer present in the basic form: (a) HCO_3^-/CO_3^{2-} buffer; (b) $H_2PO_4^-/HPO_4^{2-}$ buffer.

general base catalysis while those obtained with carbonate and phosphate ($H_2PO_4^-/HPO_4^{2-}$) buffer exhibit both general base and general acid catalysis. The observed rate constants can, therefore, be expressed as in eqs 9 and 10, where k_{ly} is the rate of the lyate

$$k_{obsd} = k_{ly} + k_{gb}\frac{K_a}{K_a + a_H}[B]_T \quad (9)$$

$$k_{obsd} = k_{ly} + k_{gb}\frac{K_a}{K_a + a_H}[B]_T + k_{ga}\frac{a_H}{K_a + a_H}[B]_T \quad (10)$$

species catalyzed reaction ($k_{ly} = k_{obsd}$ in eq 7), k_{gb} and k_{ga} are the second-order rate constants for general base and general acid catalysis, K_a is the acid dissociation constant of the buffer, and $[B]_T$ is the total concentration of buffer species present, i.e., [HB] + [B]. Plots of k_{obsd} vs. $[B]_T$ (Figure 3) give slopes that, when divided by the mole fraction of buffer present in the basic form $K_a/(K_a + a_H)$, give values of k_{gb} if only general base catalysis is occurring and values of $k_{gb} + k_{ga}a_H/K_a$ if both general base and general acid catalysis are operative. In the case of the latter, values of k_{gb} and k_{ga} are obtained from the intercepts and slopes, respectively, of secondary plots of slope/(K_a/(K_a + a_H)) vs. a_H/K_a.

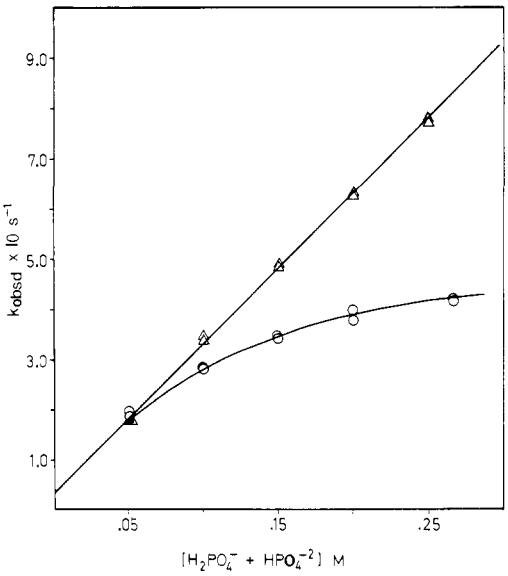

Figure 5. Plots of the observed first-order rate constants for the reaction of oxaloacetic acid with phosphate at pH 5.64 vs. the total concentration of phosphate buffer: (Δ) rate constants obtained from pH decrease experiments using oxaloacetic acid initially equilibrated at pH 12.3; (O) rate constants obtained from pH increase experiments using oxaloacetic acid initially equilibrated at pH 2.2.

The secondary plots obtained with carbonate and phosphate buffers are shown in Figure 4.

The observed rate constants of eq 9 and 10 were determined by mixing a solution of oxaloacetate initially equilibrated at pH 2.2 with a solution of the oxygen base (at a pH within ±1 of its pK_a allowing it to act as its own buffer) and monitoring the increase in absorbance and also by mixing an oxaloacetate solution at pH 12.3 with the same buffer solution and monitoring the decrease in absorbance. With phosphate (pK_a = 11.35) and carbonate (pK_a = 9.78) buffers, the observed rate constants determined for the pH increase experiments are identical with those obtained for the pH decrease experiments (Figure 3), and the intercepts of the linear buffer dilution plots at zero buffer concentration fall on the pH rate profile for enolization shown in Figure 2 (indicated by solid circles).

For the reaction of oxaloacetic acid with phosphate buffer in the pH range of the second pK_a of phosphate (pK_a = 6.70), linear buffer dilution plots were obtained only from the pH decrease experiments. The pH increase experiments result in nonlinear buffer dilution plots (Figure 5). Only at low buffer concentrations are the rates from the pH increase and pH decrease experiments identical. As the buffer concentration is increased, hydration becomes rate limiting for the pH increase experiments, resulting in a change in slope of the buffer dilution plot. Enolization apparently remains rate limiting at all buffer concentrations for the pH decrease experiments. When, however, the buffer dilution plots of the pH decrease experiments are extrapolated to zero buffer concentration, the intercepts exhibit a positive deviation from the enolization pH–rate profile of Figure 2 (solid circles in the pH range 6.7–7.3). This suggests that there is some contribution to the observed rate constant from perturbation of the hydration equilibrium. This contribution is sufficiently small not to affect the linearity of the buffer dilution plots. Thus the reported percentage of hydrate at pH 6.7 in Table I, indicating that there is no change in hydrate concentration as the pH is decreased from pH 12.3 to 6.7, must be in error.

The logs of the k_{gb} values of eq 9 and 10 are plotted (solid squares) in Figure 6 vs. the pK_a of the catalyst. These values result in a Brønsted β value of 0.32 for the oxygen base catalyzed enolization of oxaloacetic acid. The second-order rate constants in Figure 6 are numbered to correspond to the numbers assigned to the catalysts in Tables II and III.

In the presence of oxygen bases, the pH decrease experiments evidence an initial rapid decrease in absorbance prior to the de-

Table II. Second-Order Rate Constants (M^{-1} s^{-1}) for the Reaction of a Variety of Catalysts with Oxaloacetic Acid

catalyst	pK_a	k_{gb}	k_{ga}	k'_{ga}
(1) HO^-/H_2O	15.75	73.5		1.24×10^{-1}
(2) PO_4^{3-}/HPO_4^{2-}	11.35	8.00		67.0
(3) 2-(diisopropylamino)ethanol	10.25	3.06		285
(4) CO_3^{2-}/HCO_3^-	9.77	6.82×10^{-1}	2.33×10^{-1}	317
(5) $HPO_4^{2-}/H_2PO_4^-$	6.70	1.10×10^{-1}	2.28	

Table III. Second-Order Rate Constants (M^{-1} s^{-1}) for the Reaction of Tertiary Amines with Oxaloacetic Acid

tertiary amine	pK_a	k_{1N}	k_{1NH}	k_{2N}	k_{2NH}	k_{3NH}	k_{4N}	k_{4NH}
(6) quinuclidine	11.22			94		6 000	1770	
(7) triethylamine	10.80					2 300	211	
(8) trimethylamine	10.08	1240		13		54 300	925	
(9) 3-quinuclidinol	10.02	1230		12		60 400	794	
(10) *N,N,N',N'*-tetramethylethylenediamine	9.42	615				154 000	408	
(11) 1,4-diazabicyclo[2.2.2]octane	8.99	783		3.2		331 000	400	
(12) 3-chloroquinuclidine	8.90	224		2.3			197	
(13) *N,N,N',N'*-tetramethylethylenediamine-H^+	6.22	152	75	2.0	3.5		88	31

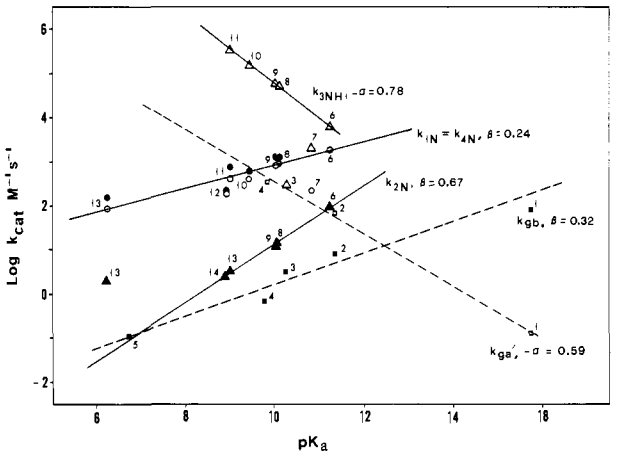

Figure 6. Dashed lines: Brønsted plots obtained for the reaction of oxaloacetic acid with oxygen bases and 2-(diisopropylamino)ethanol; (□) second-order rate constants (k'_{ga} of eq 11) for general acid-catalyzed protonation of enolate anion; (■) second-order rate constants (k_{gb} of eq 9 and 10) for general base catalyzed enolization. Solid lines: Brønsted plots obtained for the reaction of oxaloacetic acid with tertiary amines; (▲) second-order rate constants for general base catalyzed dehydration; second-order rate constants for tertiary amine catalyzed enolization obtained from (●) pH increase and pH decrease (○) experiments; (△) second-order rate constants for the initial rapid general acid catalyzed reaction observed in the pH decrease experiments.

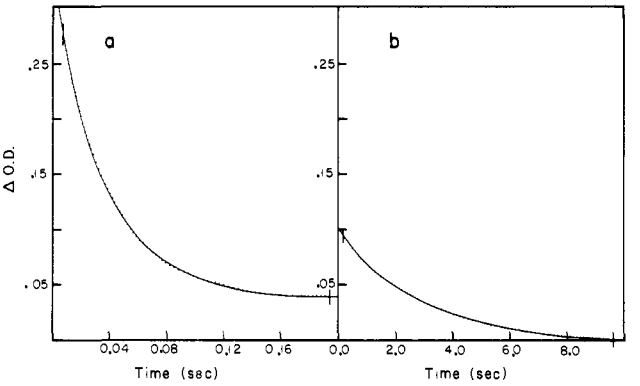

Figure 7. Stopped-flow traces for the two rate processes observed in pH decrease experiments for the reaction of oxaloacetic acid with carbonate buffer at pH 10.52: (a) data points collected during the first 0.2 s after mixing; (b) data points collected during the first 10 s after mixing. The points are experimental; the lines were computer generated using points within the boundaries of the vertical tics and give rise to computer-generated rate constants of 27.7 and 3.41×10^{-1} s^{-1}, respectively.

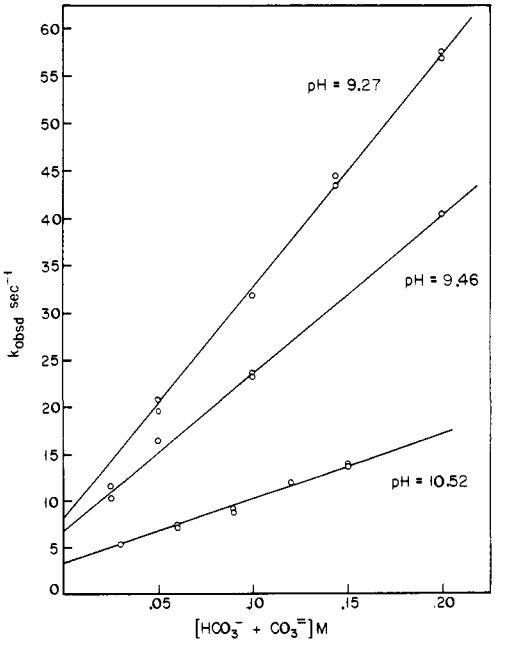

Figure 8. Plots of the first-order rate constants for the initial rapid reaction of oxaloacetic acid in the presence of carbonate buffer observed in the pH decrease experiments vs. the total concentration of carbonate buffer at three pH values.

crease in absorbance associated with keto–enol interconversion. The stopped-flow traces for the two rate processes are shown in Figure 7 for the reaction of oxaloacetate with carbonate buffer; data points were collected over a 0.2-s interval for the initial reaction and over 10 s for the subsequent enolization reaction. Computer-generated lines were drawn through the data points and give computer-generated rate constants of 2.77×10 s^{-1} and 3.41×10^{-1} s^{-1} for the two rate processes. (The rate constants for the slower of the two rate processes are plotted in Figure 3.) The initial reaction is observed when oxaloacetate is initially equilibrated at pH 12.3 (i.e., in the pH decrease experiments). It is not observed when oxaloacetate is equilibrated at pH 2.2 and subsequently made more basic. Buffer dilution plots obtained for this initial rapid reaction with oxygen bases evidence general acid catalysis (Figure 8). The observed rate constants can, therefore, be expressed as in eq 11. The intercepts of the buffer dilution

$$k_{obsd} = k'_{1y} + k'_{ga}\frac{a_H}{K_a + a_H}[B]_T \qquad (11)$$

plots (k'_{1y}) fall on the dotted line of Figure 2 (indicated by solid triangles), which were drawn through the rate constants observed for the initial rapid reaction observed in the pH decrease experiments in the presence of lyate species, attributed to protonation of enolate anion. The amplitude of the absorbance change associated with the initial reaction is more than twice that associated with the subsequent enolization reaction (Figure 7a, OD = 0.237;

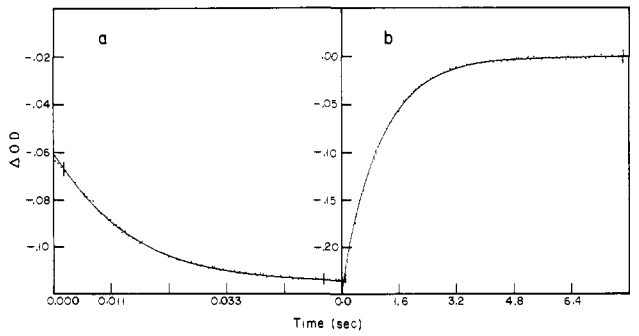

Figure 9. Stopped-flow traces for the two rate processes observed in pH increase experiments for the reaction of oxaloacetic acid with trimethylamine at pH 9.41: (a) data points collected during the first 0.055 s after mixing; (b) data points collected during the first 8.0 s after mixing. The points are experimental; the lines were computer generated using points within the boundaries of the vertical tics and give rise to computer-generated rate constants of 69.0 and 9.37 × 10^{-1} s^{-1}, respectively.

Figure 7b, OD = 0.097). The observation of the initial reaction only in the pH decrease experiments, the values of the intercepts of the buffer dilution plots, and the relatively large absorbance change all suggest that this reaction may be attributed to general acid catalyzed protonation of enolate anion. The second-order general acid catalyzed rate constants (open squares in Figure 6) give a Brønsted $-\alpha$ value of 0.59. The Brønsted plots of Figure 6 pertaining to the reaction of oxaloacetic acid with oxygen bases are indicated by dashed lines while solid lines are used to designate those plots that pertain to the reaction with tertiary amines. All second-order rate constants associated with the reaction of oxaloacetic acid with oxygen base catalysts are given in Table II.

Catalysis by Tertiary Amines. The enolization of oxaloacetic acid was investigated in the presence of tertiary amines. The amines employed are listed in Table III. The change in the equilibrium distribution of keto, enol, and hydrate occurring as a result of a rapid increase in pH and after a rapid decrease in pH were both monitored. The average pH of the reaction mixtures obtained from the pH decrease experiments agreed with the average pH of the reaction mixtures obtained from the pH increase experiments within about 0.05 pH unit.

For the pH increase experiments, the oxaloacetic acid solution was initially adjusted to pH 2.2. Upon mixing with amine, the pH immediately increased to that of the buffered amine solution. As a result of this pH increase, a biphasic reaction is observed as the oxaloacetate equilibrates to a new distribution of keto, enol, and hydrate. Initially there is a rapid decrease in absorbance which is followed by a slower absorbance increase. The rates of the two successive first-order relaxations are sufficiently different that they can be calculated independently (see Experimental Section). A typical stopped-flow trace is shown in Figure 9. The solutions are mixed, and the points collected during the first 0.055 s of the reaction are shown in Figure 9a. The reaction is again initiated, and the points collected during the first 8.0 seconds after mixing are shown in Figure 9b. The lines through the points were computer generated and result in rate constants of 6.90 × 10 and 9.37 × 10^{-1} s^{-1} for the two rate processes. The absorbance change associated with the second slower relaxation is about 5 times greater than that of the initial rapid relaxation. From the relative absorbance changes, it is apparent that the initial rapid reaction is attributable to keto–enol interconversion and the second slower reaction to keto–hydrate interconversion (see Discussion). Stopped-flow traces similar to those in Figure 9 were obtained from the pH increase experiments of oxaloacetic acid with all the tertiary amines (except triethylamine, see below) listed in Table III.

When the observed first-order rate constants for the initial rapid reaction characterized by decreasing absorbance (Figure 9a) are plotted vs. the concentration of amine (with amine concentration ranging from 0.025 to 0.25 M), buffer dilution plots such as those shown in Figure 10 are obtained. A minimum of five buffer dilution plots, each at a different pH, were obtained for each

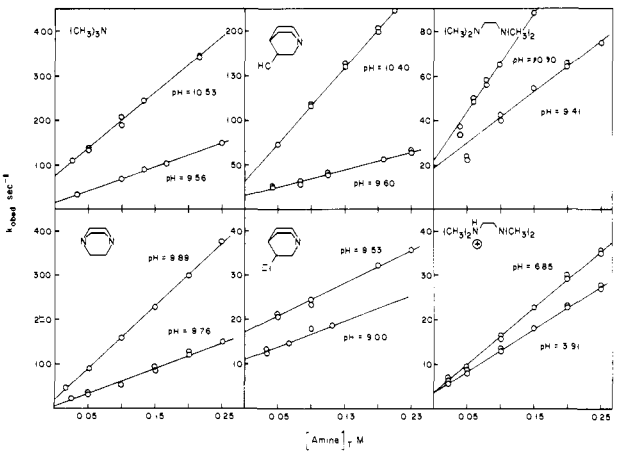

Figure 10. Plots of the observed first-order rate constants, obtained from pH increase experiments, for the initial rapid reaction (enolization) of oxaloacetic acid with a tertiary amine (k_{1N}) vs. the total concentration of tertiary amine. Data for six different tertiary amines are shown.

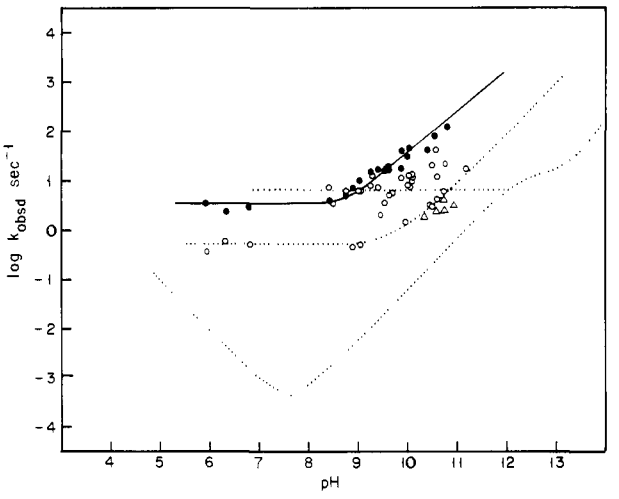

Figure 11. Dotted lines correspond to the three pH–rate profiles of Figure 2. Intercepts (●) of tertiary amine buffer dilution plots at zero amine concentration obtained from pH increase experiments (k_{1N}); intercepts (○) of tertiary amine buffer dilution plots at zero amine concentration obtained from pH decrease experiments (k_{4N}) for all the tertiary amines listed in Table III except triethylamine; intercepts (△) at zero amine concentration of triethylamine buffer dilution plots obtained from pH decrease experiments .

tertiary amine; at least 12 rate constants were determined for each buffer dilution plot. All of these plots are linear and support catalysis by amine free base, except in the case of *N,N,N′,N′*-tetramethylethylenediamine–H^+, the least basic of the tertiary amines employed, where catalysis by both the acid and base form of the amine is evident. The second-order rate constants, k_{1N} and k_{1NH}, calculated by employing eq 9 and 10 where $k_{gb} = k_{1N}$, $k_{ga} = k_{1NH}$, and $[B]_T = [N] + [NH]$, are listed in Table III. Extrapolation of the buffer dilution plots of Figure 10 to zero amine concentration results in intercept values that correspond neither to the rate of keto–enol interconversion nor to the rate of keto–hydrate interconversion in the presence of lyate species at the same pH. The pH–rate profiles shown in Figure 2 for enolization, dehydration, and enolate protonation are reproduced in Figure 11, and the intercepts of the buffer dilution plots for the initial rapid reaction in the presence of tertiary amines are plotted (solid circles) as a function of the pH at which each was obtained. The solid line drawn through these intercept values was computer generated from eq 12, where $k'_0 = 3.44$ s^{-1}, $k''_{HO^-} = 1.94 \times 10^5$

$$k_{obsd} = k'_0 + k''_{HO^-}K_w/a_H \qquad (12)$$

M^{-1} s^{-1}, and $pK_w = 13.83$. The intercept values are about 10 times greater than the dehydration rate constants and more than 500 times greater than the enolization rate constants.

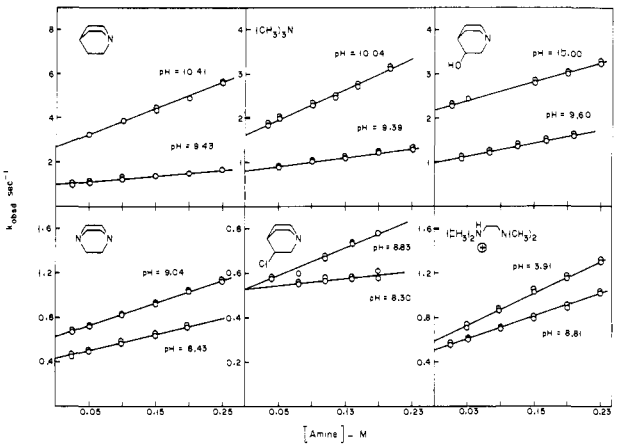

Figure 12. Plots of the observed first-order rate constants, obtained from pH increase experiments, for the second slower reaction (dehydration) of oxaloacetic acid with a tertiary amine (k_{2N}) vs. the total concentration of tertiary amine. Data for six different tertiary amines are shown.

In Figure 12 are shown plots of the observed first-order rate constants for the second slower reaction observed in the presence of tertiary amines (Figure 9b) as a function of total amine concentration. As was observed for the initial reaction, the plots are linear and, except for *N,N,N',N'*-tetramethylethylenediamine–H^+, support catalysis only by amine free base. The second-order rate constants, k_{2N} and k_{2NH}, are given in Table III; the logs of the k_{2N} values are plotted in Figure 6 (solid triangles) and result in a Brønsted β value of 0.67. The intercepts of the buffer dilution plots of Figure 12 at zero amine concentration fall on the dashed line of Figure 2 (solid squares) confirming that this second slower reaction may be attributed to amine catalysis of keto–hydrate interconversion.

Since the intercept values of the buffer dilution plots for the initial rapid reaction associated with the pH increase experiments (Figure 11) are so much greater than can be accounted for by lyate species catalyzed enolization or dehydration, the reaction was reinvestigated at very low amine concentration. At low amine concentration the amine cannot be expected to maintain constant pH upon addition of acidic oxaloacetate. Since the reaction is much slower in the presence of oxygen bases than it is in the presence of tertiary amines, carbonate buffer was used to maintain the desired pH. All the amines listed in Table III were investigated, each at ten different amine concentrations ranging from 0.000833 to 0.0833 M and each containing 0.20 M total carbonate buffer. Representative buffer dilution plots for the reaction of oxaloacetic acid with 3-quinuclidinol are shown in Figure 13; each of the tertiary amines investigated gave essentially identical results. The pH of the buffered solutions after mixing with an oxaloacetic acid solution at pH 2.2 all agreed within ±0.03 pH unit as indicated in the inset to Figure 13b. The initial rate characterized by decreasing absorbance is observable only at the five highest amine concentrations (0.0167–0.0833 M). These rate constants are plotted vs. amine concentration in Figure 13a. The slope and intercept values are identical with those previously obtained at higher amine concentration in the absence of carbonate buffer (e.g., Figure 10). At intermediate amine concentrations (0.0083–0.0120 M), the initial reaction is observable only as a lag phase before the second slower reaction, and rate constants cannot be accurately calculated. At the lowest amine concentrations (<0.0083 M), the initial rapid reaction is not observed. The second slower reaction characterized by increasing absorbance is observed at all amine concentrations (Figure 13b). Only at high amine concentrations, however, are the rate constants linearly dependent on amine concentration. At low amine concentrations there is a marked negative deviation from linearity with the rate constants approaching the rate observed in the presence of 0.2 M carbonate with no added amine (shown on the *y* axis). The slope of the linear portion of the buffer dilution plot is identical with the slope previously obtained at higher amine (0.025–0.25 M) concentrations (e.g., Figure 12), and the line extrapolates to

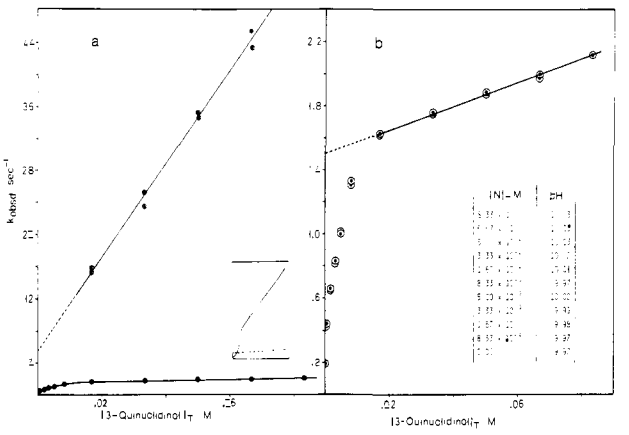

Figure 13. Observed first-order rate constants, obtained from pH increase experiments, for the reaction of oxaloacetic acid with 3-quinuclidinol vs. the total concentration of 3-quinuclidinol. All amine solutions contain 0.2 M carbonate buffer: (a) rate constants for the initial rapid reaction; (b) rate constants for the subsequent slower reaction. For the sake of comparison the data of b are replotted in a. Inset to a: schematic diagram showing the intersection of the buffer dilution plot for enolization (solid line) and that for dehydration (dashed line). Inset to b: concentration and pH of each of the amine buffer solutions employed for the data of a and b.

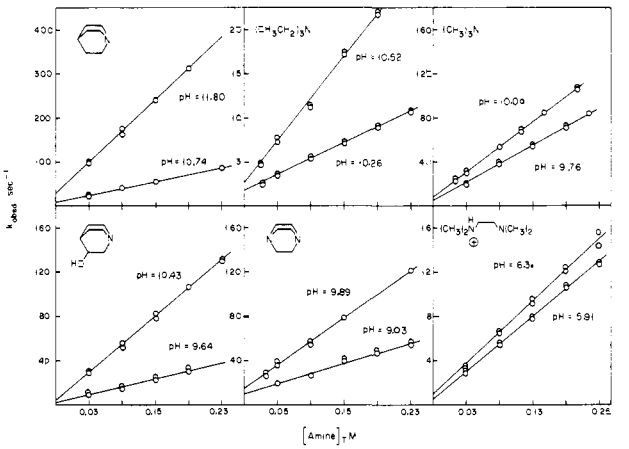

Figure 14. Plots of the observed first-order rate constants, obtained from pH decrease experiments, for the reaction (enolization) of oxaloacetic acid with a tertiary amine (k_{4N}) vs. the total concentration of tertiary amine. Data for six different amines are shown.

an intercept value that falls, as expected, on the dashed line of Figure 2. The buffer concentrations employed for the data of Figure 13 and the pH values of the final reaction mixtures are shown in the inset to Figure 13b. Thus the nonlinearity of the buffer dilution plot cannot be attributed to lack of pH control. The data shown in Figure 13b are reproduced in Figure 13a in order to show both rate processes on the same scale.

For the pH decrease experiments, the oxaloacetic acid solution was initially adjusted to pH 12.3. The pH instantaneously decreased to the pH of the buffered amine solution upon mixing with amine. As a result of the decrease in pH, a single first-order rate process, characterized by decreasing absorbance, is observed as the keto, enol, and hydrate forms of oxaloacetic acid reequilibrate. Plots of the observed rate constants vs. amine concentration (with amine concentration ranging from 0.025 to 0.25 M) were obtained for each of the amines listed in Table III. A minimum of five buffer dilution plots were obtained for each amine, each at a different pH; some of these plots are shown in Figure 14. The rate constants observed as a result of a rapid decrease in pH exhibit an apparent linear dependence on amine concentration. The second-order rate constants, k_{4N} and k_{4NH}, determined from these plots by employing eq 9 and 10 where $k_{gb} = k_{4N}$, $k_{ga} = k_{4NH}$, and $[B]_T = [N] + [NH]$ are listed in Table III. Similar to what was found from the pH increase experiments, catalysis only by amine

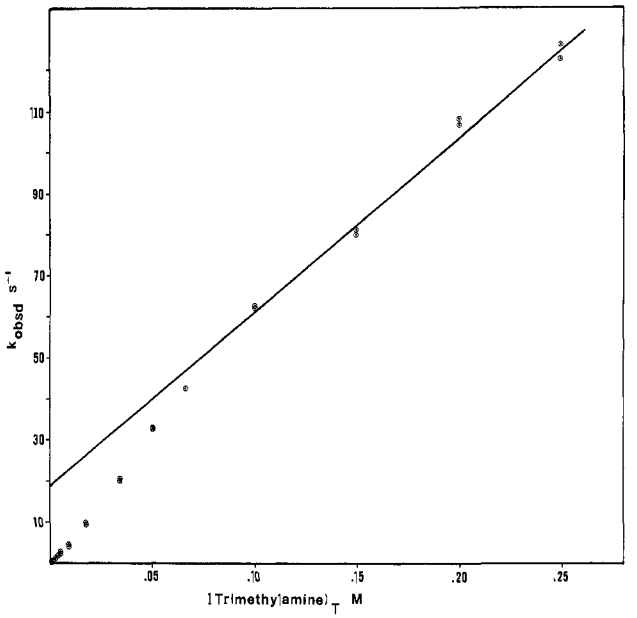

Figure 15. Observed first-order rate constants, obtained from pH decrease experiments, for the reaction of oxaloacetic acid with trimethylamine at pH 10.10 vs. the total concentration of trimethylamine. All amine solutions <0.05 M in amine contain 0.2 M carbonate buffer. The points representing rate constants at amine concentrations <0.07 M are duplicates.

free base is observed for the first seven amines listed in Table III, while catalysis by both amine free base and protonated amine occurs with the least basic of the tertiary amines. The logs of the intercept values obtained by extrapolating the buffer dilution plots of Figure 14 to zero amine concentration are plotted in Figure 11 (open circles). These intercept values are similar to the ones (solid circles) obtained from buffer dilution plots of the initial reaction observed in the pH increase experiments (Figure 10). The second-order rate constants (k_{4N} and k_{4NH}) obtained from the single reaction observed in the pH decrease experiments are also not very different from the second-order rate constants obtained from the first of the two successive reactions observed in the pH increase experiments (k_{1N} and k_{1NH}). These second-order rate constants are plotted in Figure 6 (k_{1N} indicated by solid circles and k_{4N} indicated by open circles) and give a Brønsted β value of 0.24. Although the second-order rate constants obtained from the pH decrease reaction (k_{4N}) are comparable to those obtained from the first of the two rate processes observed in the pH increase reaction (k_{1N}), it should be noted that the first-order rate constants obtained from the pH decrease reaction are not identical with either of the two first-order rate constants observed in the pH increase experiments. They are somewhat slower than those obtained for the rapid initial reaction and very much larger than those obtained for the second slower reaction. From comparison of the observed rate constants determined at 0.2 M total amine, the rate of the initial reaction occurring after a rapid increase in pH is from 1.3 to 2.9 times faster than the single reaction observed after a rapid decrease in pH, although the pH of the reaction mixture is essentially the same in both experiments.

Since the intercepts of the buffer dilution plots of the pH decrease reactions are similar to those found for the first of the reactions occurring after a rapid increase in pH, the buffer dilution plots of Figure 14 were extended to very low tertiary amine concentrations using 0.2 M carbonate buffer to maintain constant pH. The results obtained from the reaction of oxaloacetic acid with trimethylamine, investigated over a concentration range of 0.000 83–0.25 M $[N]_T$, are shown in Figure 15. The first-order dependence on tertiary amine concentration observed at high amine concentration is not maintained at very low amine concentrations. All the tertiary amines listed in Table III showed similar behavior; the apparent first-order dependence on amine concentration exhibited in Figure 14, which gives rise to unexpectedly large intercept values, does not hold up when the buffer dilution plots are expanded to include rate constants obtained at low amine concentration. There is a negative deviation from the line established for the first-order tertiary amine dependence with the rate constants approaching the value for carbonate catalyzed enolization at zero amine concentration.

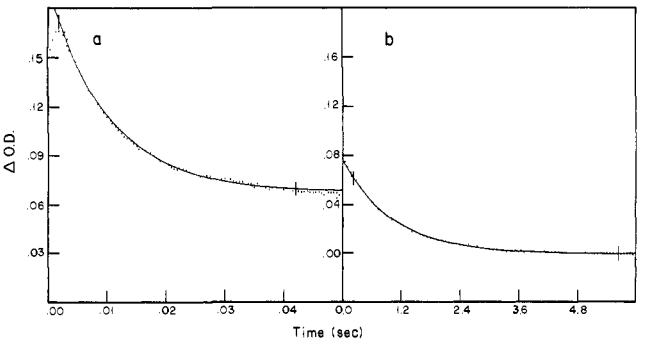

Figure 16. Stopped-flow traces for the two reactions observed in pH decrease experiments for the reaction of oxaloacetic acid with 0.001 67 M trimethylamine at pH 10.16: (a) data points collected during the first 0.05 s after mixing; (b) data points collected during the first 6.0 s after mixing. The points are experimental; the lines were computer generated using points within the boundaries of the vertical tics and give rise to computer-generated rate constants of 98.3 and 9.67 × 10^{-1} s^{-1}, respectively.

Investigations of the pH decrease reaction at very low tertiary amine concentrations led to the observation of a rate process that was not previously observed in the pH decrease reactions. It is a very rapid reaction, too rapid to be observed at amine concentrations greater than ~0.008 M. It is characterized by decreasing absorbance, occurring before the decrease in absorbance associated with the rate process plotted in Figures 14 and 15. The stopped-flow traces associated with the two reactions are shown in Figure 16 for the reaction of oxaloacetic acid with trimethylamine. In Figure 16a are shown the points collected during the first 0.05 s after mixing; the reaction was reinitiated, and the points obtained within 6.0 s after mixing are shown in Figure 16b. Computer-generated lines are drawn through the experimental points and give rise to rate constants of 9.83 × 10 and 9.67 × 10^{-1} s^{-1} for Figure 16, parts a and b, respectively. The rate process shown in Figure 16b corresponds to the rate constants plotted in Figure 14. The absorbance change associated with the initial reaction is about 1.3 times greater than that of the subsequent slower reaction. Representative buffer dilution plots obtained for the initial rapid reaction observed at low amine concentration in the pH decrease experiments are shown in Figure 17. These plots evidence a first-order dependence on amine concentration and support catalysis by protonated amine. The second-order rate constants, k_{3NH}, obtained from such plots are listed in Table III; they are plotted (open triangles) in Figure 6 and give a Brønsted α value of −0.78. This reaction occurs too rapidly to be detected with amines of pK_a less than 9.

The magnitude of the absorbance change associated with this initial rapid reaction, the observation of general acid catalysis, and the Brønsted $-\alpha$ value suggest that the reaction is most likely attributable to protonation of enolate anion. The large slopes associated with the buffer dilution plots of Figure 17 make it difficult to determine accurate values for the rate constants at zero amine concentration. These intercepts have an approximate value of 40 ± 15 s^{-1}. Given the observed value of 6.7 s^{-1} (eq 9) for water-catalyzed enolate anion protonation and the second-order rate constant of 317 M^{-1} s^{-1} (Table II) for enolate protonation by bicarbonate, the observed intercept values (at zero amine concentration and 0.2 M $[carbonate]_T$) support the attribution of the initial rapid general acid catalyzed reaction to enolate anion protonation.

In order to compare the relative values of the rate constants obtained for the two rate processes observed in the pH increase experiments and the two rate processes observed in the pH decrease experiments when oxaloacetic reacts with tertiary amines, the rate

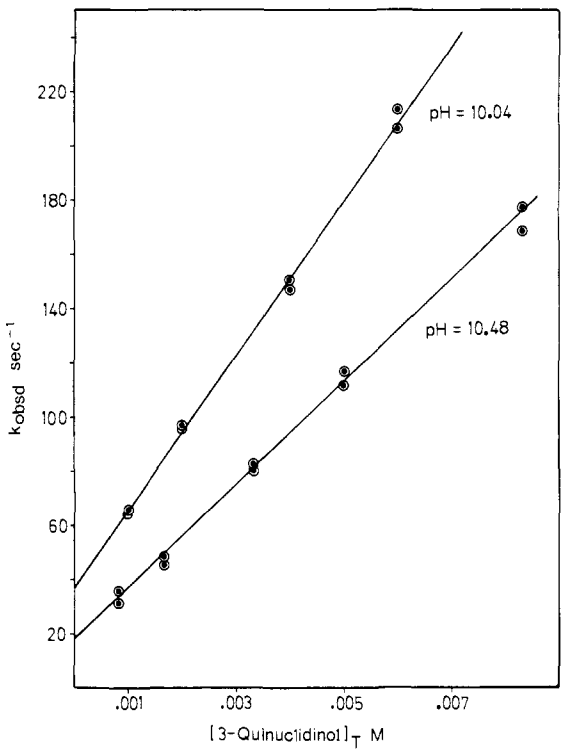

Figure 17. Plots of the observed first-order rate constants, obtained from pH decrease experiments, for the initial rapid reaction (k_{3NH}) of oxaloacetic acid with 3-quinuclidinol vs. the total concentration of 3-quinuclidinol at two pH values. All amine solutions contain 0.2 M carbonate buffer.

constants for the four rate processes obtained for the reaction of oxaloacetate with 3-quinuclidinol at pH 10.48 at low amine concentration are plotted in Figure 18. Solid lines are drawn through the rate constants obtained from the pH increase experiment and dashed lines through the rate constants obtained from the pH decrease experiment. Lines a–d correspond to the rate processes shown in Figures 17, 10, 14, and 12, respectively.

With the exception of triethylamine, the tertiary amines listed in Table III possess minimum steric hindrance. The results obtained from the pH decrease experiments with the more sterically hindered triethylamine are similar to the results obtained with the other tertiary amines; an initial general acid catalyzed reaction is observed, which is then followed by a slower reaction catalyzed by amine free base. Because of the steric hindrance associated with this amine, the second-order rate constants for the two rate processes each exhibit a negative deviation of about 0.75 log unit from the Brønsted plots associated with the reactions (Figure 6). For the pH increase experiments, the results obtained with triethylamine differ somewhat from those obtained with other tertiary amines under similar conditions; the initial rapid decrease in absorbance appears only as a lag phase proceeding a reaction that exhibits a nonlinear dependence on amine concentration. Because of the depressed rate of catalysis of keto–enol interconversion exhibited by this sterically hindered amine, the rates of triethylamine catalyzed keto–enol and keto–hydrate interconversion are not separable, and the buffer dilution plots for the pH increase reaction evidence the curvature that is observed with phosphate buffer (Figure 5). Since keto–hydrate interconversion does not play a major role in the pH decrease experiments, the behavior of triethylamine is similar to that of the other tertiary amines under the same conditions.

The enolization of oxaloacetic acid was also investigated using 2-(diisopropylamino)ethanol as a catalyst. This very sterically hindered amine does not exhibit the kinetic behavior observed for the reaction of oxaloacetic acid with the tertiary amines listed in Table III. Instead, 2-(diisopropylamino)ethanol reacts with oxaloacetic acid in the same manner as do oxygen base catalysts: (a) no initial rapid reaction is observed in the pH increase experiments; (b) the buffer dilution plots obtained from the single reaction observed as a result of a rapid increase in pH are superimposable on the buffer dilution plots obtained from the slower of the two reactions observed in the pH decrease experiments; (c) the second-order rate constant obtained from such plots falls on the Brønsted plot defined by the oxygen base catalysts (Figure 6); (d) the logs of the intercepts of these buffer dilution plots fall on the pH–rate profile for lyate species catalyzed enolization (◐ on the solid line of Figure 2).

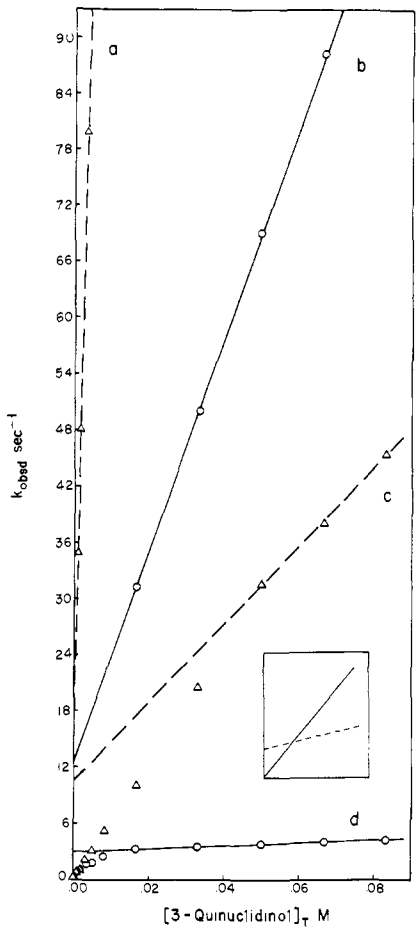

Figure 18. Plots of the observed first-order rate constants for the reaction of oxaloacetic acid with 3-quinuclidinol at pH 10.48 vs. the total concentration of 3-quinuclidinol. Solid lines are drawn through rate constants determined from pH increase experiments: line b is the initial rapid reaction that evidences decreasing absorption (k_{1N}) and line d the subsequent slower reaction that evidences increasing absorption (k_{2N}). Dashed lines are drawn through rate constants determined from pH decrease experiments: line a is the initial rapid general acid catalyzed reaction (k_{3NH}) and line c the subsequent slower reaction (k_{4N}). Inset: schematic diagram (according to Emly and Leussing[6]) showing the intersection of the buffer dilution plot for enolization (solid line) and that for dehydration (dashed line).

Discussion

Composition of Oxaloacetic Acid. In aqueous solution keto oxaloacetic acid exists in equilibrium with its hydrate and enol (enolate) forms (eq 4). At 270 nm, the wavelength at which the rates of interconversion of the various forms was monitored, only enol and enolate have any significant absorbance. For the pH increase experiments, aqueous oxaloacetic acid was initially equilibrated at pH 2.2 and then mixed with a more basic buffered solution, resulting in a rapid increase in pH to that of the buffered solution. At pH 2.2 the [enol]/[ketone] ratio is ~0.3 and the [hydrate]/[ketone] ratio is >1.0 (Table I). When the acidic substrate is injected into basic solutions where the [enol]/[ketone] ratio is 0.14 and the [hydrate]/[ketone] ratio is 0.08, the rate process(es) observed will depend on the relative rates of keto–enol and keto–hydrate interconversion.

If keto–enol interconversion is more rapid than keto–hydrate interconversion, there will be an initial loss of absorbance as enol is converted to ketone to shift the [enol]/[ketone] ratio from 0.3 to 0.14. This will then be followed by the slower conversion of hydrate to ketone as the [hydrate]/[ketone] ratio decreases from >1.0 to 0.08. This normally spectrally unobservable reaction can be monitored by the rate of increase in absorbance due to the rapid formation of enol, which will follow the rate-limiting conversion of hydrate to ketone. The absorbance change associated with the second reaction will be greater than that associated with the initial reaction since the shift in equilibrium precipitated by the change in pH is greater for the [hydrate]/[ketone] equilibrium than for the [enol]/[ketone] equilibrium (Figure 9).

If, on the other hand, keto–hydrate interconversion is more rapid than keto–enol interconversion, the initial conversion of hydrate to ketone will be spectrally unobservable. The only rate process that will be seen will be the subsequent slower conversion of ketone to enol, which will be characterized by increasing absorbance.

For the pH decrease experiments, aqueous oxaloacetate was initially equilibriated at pH 12.3. Mixing with a buffered solution of lower pH results in an instantaneous decrease in pH to that of the buffered solution. The data of Table I suggest that there is no significant change in hydrate concentration as the basic oxaloacetate solution is mixed with buffers of pH >6. Thus, the only rate process expected to occur is the conversion of enol and enolate to ketone, which will be characterized by decreasing absorbance.

Catalysis by Lyate Species. The solid line of Figure 2 is drawn through the rate constants obtained for the lyate species catalyzed interconversion of the keto and enol tautomers of oxaloacetic acid. Lyate species catalysis of keto–hydrate interconversion is shown by the dashed line in the same figure. The pH-independent first-order rate constant of 0.57 s^{-1} obtained (eq 8) for water-catalyzed dehydration at 30 °C is close to the value of 0.48 s^{-1} reported by Pogson and Wolfe for the rate of dehydration in 0.1 M phosphate at 20 °C.[13] Since at all pH values the rate of keto–hydrate interconversion is faster than that of keto–enol interconversion in the presence of lyate species, only the enolization reaction is observed spectrally.

At a given pH the observed rate constant (k_{obsd}) for the interconversion of keto and enol tautomers is given by the sum of the forward (k_f) and reverse (k_r) rate constants since an approach to an equilibrium position is involved. Thus, at any constant pH, identical rate constants are obtained when employing an acidic stock solution of oxaloacetate to monitor the increase in absorbance associated with overall enolization and when using a basic stock solution of substrate to monitor the decrease in absorbance attributable to overall ketonization.

The specific acid catalyzed pathway for enolization occurring below pH 7 is attributable to preequilibrium protonation of ketone followed by removal of the α-proton by water (eq 1 with B = H_2O and HB = H_3O^+). The rate-determining step of eq 1 may be assumed to be proton removal from carbon in the forward direction and proton donation to carbon in the reverse direction since proton donation to and from oxygen may be assumed to be rapid and to be controlled by the pH of the solution and the pK_a of protonated ketone. Thus the kinetic expression for the mechanism of eq 1 may be described by the rate law of eq 13, where K_E and

$$k_{obsd} = k_f + k_r = k_2[H_2O]\left(\frac{a_H}{K_K + a_H}\right) + k_{-2}a_H\left(\frac{a_H}{K_E + a_H}\right) \quad (13)$$

K_K are the acid dissociation constants of enol and protonated ketone, respectively. Since in the investigated acid pH range, $K_K > a_H$ and $a_H > K_E$, eq 13 can be simplified to give eq 14.

$$k_{obsd} = k_f + k_r = \left(\frac{k_2}{K_K}[H_2O] + k_{-2}\right)a_H \quad (14)$$

(13) Pogson, C. I.; Wolfe, R. G. *Biochem. Biophys. Res. Commun.* **1972**, *46*, 1048.

In solutions of pH >7 the mechanism of eq 2, with B = HO^- and HB = H_2O, is followed. As under acidic conditions, the rate-limiting step in the forward and reverse directions may be assumed to be proton removal from and proton donation to the α-carbon atom, respectively. The observed rate constant under basic conditions is described by the rate law of eq 15. Summation

$$k_{obsd} = k_f + k_r = k_1[HO^-] + k_{-1}[H_2O]K_E/(K_E + a_H) \quad (15)$$

of eq 14 and 15 results in the empirical expression of eq 7 which was used to generate the solid line pH–rate profile of Figure 2.

In the presence of lyate species a rapid initial reaction, occurring in the pH decrease experiments before the reaction ascribed to enolization, is also observed. This reaction, described by the dotted line in Figure 2, is attributed to protonation of enolate anion by water. The assignment of this reaction to enolate anion protonation is based on the relatively large change in absorbance associated with the reaction compared to the absorbance change of the subsequent enolization reaction, the observation of the reaction only in the pH decrease experiments, and the similarity in value of the rate of the water catalyzed reaction and the $k_{-1}[H_2O]$ term of eq 15 (see Results).

Catalysis by Oxygen Bases. In the presence of oxygen base buffers such as carbonate and phosphate, the interconversion of keto and enol tautomers is subject to general catalysis. The buffer dilution plots obtained with phosphate (pK_a = 11.35) and carbonate buffer are linear (Figure 3); the former evidences only general base catalysis, and the latter exhibits both general acid and general base catalysis (Figure 4). Since keto–hydrate interconversion is faster than keto–enol interconversion in the presence of these buffers, only the enolization reaction is observed. The enolization rate constants obtained from the pH increase experiments are identical with the enolization rate constants obtained from the pH decrease experiments. In the case of phosphate buffer (pK_a = 6.70), the second-order enolization and hydration rate constants are similar (Figure 6). Consequently, only the pH decrease experiments, where there is little change in the keto–hydrate equilibrium, give rise to rate constants that exhibit a linear dependence on buffer concentration (Figure 5); both general acid and general base catalysis is evident (Figure 4). Curved buffer dilution plots are obtained from the pH increase experiments since a significant perturbation of the keto–hydrate equilibrium is involved. Downward curvature is evidenced in the buffer dilution plots as the rate-limiting step changes from keto–enol interconversion to keto–hydrate interconversion. A representative buffer dilution plot is shown in Figure 5.

When the oxygen base buffer dilution plots such as those shown in Figure 3 are extrapolated to zero buffer concentration, the logs of the intercept values fall on or near the pH–rate profile for enolization determined in the presence of lyate species (solid circles on the solid line of Figure 2). That there is some perturbation of the keto–hydrate equilibrium even in the pH decrease experiments in the presence of phosphate buffer (Figure 5) is shown by the positive deviation of the intercepts of the buffer dilution plots from the enolization pH–rate profile (solid circles in Figure 2 from pH 5.7 to 7.3).

That the intercept values of oxygen base buffer dilution plots fall on or near the pH–rate profile for lyate species catalyzed enolization indicates that oxygen bases catalyze the enolization of oxaloacetic acid by the same mechanisms established for the reaction in the presence of lyate species (eq 1 and 2). Thus, when general base catalysis is observed, keto–enol interconversion proceeds by the mechanism given in eq 2 and the observed rate constant can be expressed as in eq 16, where K_A is the acid

$$k_{obsd} = k_f + k_r = k_{ly} + \left(k_1 + k_{-1}\frac{a_H}{K_A}\left(\frac{K_E}{K_E + a_H}\right)\right)[B] \quad (16)$$

dissociation constant of the buffer, [B] is the concentration of the general base, and k_{ly} is the contribution to catalysis in the forward and reverse directions by lyate species. When both general acid and general base catalyses are observed, the mechanisms of eq

1 and 2 are operating simultaneously. The general acid component of the reaction can be expressed as

$$k_{obsd} = k_f + k_l = k_{ly} + (k_2K_A/K_K + k_{-2})[HB] \quad (17)$$

where [HB] is the concentration of the general acid. The terms within the parentheses in eq 16 and 17 correspond to the k_{gb} and k_{ga} values reported in Table II. The Brønsted plot for the general base catalyzed enolization reaction is shown in Figure 6; a β value of 0.32 is obtained for oxygen base catalyzed enolization. We have previously reported a Brønsted α value of −0.43 for the general acid catalytic rate constants.[5]

Similar to what was found in the presence of lyate species, the pH decrease experiments that were carried out in the presence of oxygen base catalysts evidence a rapid reaction (Figure 7a) occurring prior to the reaction associated with enolization (Figure 7b). The buffer dilution plots that were obtained for this initial reaction are linear and evidence general acid catalysis (Figure 8); the second-order rate constants, k'_{ga}, are listed in Table II. The logs of the intercepts of the buffer dilution plots are indicated as solid triangles on the dotted line of Figure 2, which has been attributed to protonation of enolate anion by water. The value of the intercepts, the magnitude of the absorbance change (Figure 7a) compared to that for enolization (Figure 7b), the observation of general acid catalysis, and the fact that the reaction is observed only in the pH decrease experiments combine to suggest that it is attributable to general acid protonation of enolate anion. The second-order general acid catalyzed rate constants are plotted in Figure 6 (open squares) and give rise to a α value of −0.59.

Catalysis by Tertiary Amines. The interconversion of the keto–enol and keto–hydrate forms of oxaloacetic acid was investigated employing tertiary amines as catalysts. In the presence of tertiary amines, contrary to what is observed in the presence of oxygen base catalysts, keto–enol interconversion occurs more rapidly than does keto–hydrate interconversion; consequently, rate constants are obtainable for both rate processes.

In the pH increase experiments, where the substrate is initially equilibrated at pH 2.2 and thus contains a considerable concentration of hydrate, two rate processes are observed when the substrate is mixed with tertiary amine, resulting in a jump in pH to that of the tertiary amine buffer (Figure 9). Initially there is a loss of absorbance as the keto–enol equilibrium shifts in the direction of ketone (Table I). This is followed by a considerably slower increase in absorbance (Figure 9b) as the keto–hydrate equilibrium is shifted toward ketone. The rate-limiting change in the keto–hydrate equilibrium is made spectrally observable by the subsequent rapid change in the keto–enol equilibrium as a result of the increased concentration of the keto tautomer. The change in absorbance associated with the two rate processes is considerably greater for the second slower reaction. Considering the relative concentrations of ketone, enol, and hydrate present at pH 2.2 and at the pH of the tertiary amine buffers (Table I), the observed relative absorbance changes are in agreement with the assignment of the initial reaction to keto–enol interconversion and the subsequent reaction to keto–hydrate interconversion. The two successive first-order rate processes differ sufficiently in magnitude to allow each to be calculated independently (see Experimental Section).

The rate constants obtained for establishment of the keto–hydrate equilibrium, the slower of the two rate processes, exhibit a first-order dependence on tertiary amine concentration (Figure 12). The dehydration reaction is subject only to general base catalysis by tertiary amines of $pK_a > 8$ and evidences both general base and general acid catalysis by *N,N,N'N'*-tetramethylethylenediamine–H^+ ($pK_a = 6.22$). The second-order rate constants for general base catalyzed dehydration give a Brønsted β value of 0.69 (solid triangles in Figure 6). The catalytic constant for general base catalysis by *N,N,N',N'*-tetramethylethylenediamine–H^+ is approximately 50-fold greater than expected from the Brønsted plot. Presumably this is attributable to the ability of this species to act simultaneously as a general base and as a general acid catalyst (I) When the tertiary amine buffer dilution plots for keto–hydrate interconversion (such as those shown in Figure 12) are extrapolated to zero amine concentration, the logs of the intercept values fall on the pH–rate profile for dehydration (solid squares on the dashed line of Figure 2). The appropriateness of the assignment of this rate process to keto–hydrate interconversion is confirmed by the previously reported value for the rate of establishment of the hydration equilibrium of oxaloacetic acid.[13]

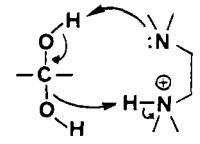

I

Some of the tertiary amine buffer dilution plots obtained for the initial rapid reaction (Figure 9a), attributed to keto–enol interconversion, are shown in Figure 10. The observed rate constants evidence an apparent linear dependence on tertiary amine concentration and, as was found in the case of keto–hydrate interconversion, the slopes of the buffer dilution plots indicate that the enolization reaction is subject only to catalysis by amine free base except in the case of *N,N,N',N'*-tetramethylethylenediamine–H^+, where both general base and general acid catalysis are apparent (Table III). The second-order rate constants for tertiary amine catalyzed enolization give a Brønsted β value of 0.24 (solid circles in Figure 6). Unlike what was found for keto–hydrate interconversion, *N,N,N',N'*-tetramethylethylenediamine–H^+ apparently does not act as an intramolecular catalyst for keto–enol interconversion.

The second-order rate constants obtained for catalysis of the enolization of oxaloacetic acid by tertiary amines are surprisingly large when compared to those obtained for catalysis by oxygen bases. Depending on the pK_a, the tertiary amine second-order rate constants are from 800 ($pK_a = 10.0$) to 2200 ($pK_a = 6.2$) times greater than the oxygen base second-order rate constants. Although tertiary amines are generally found to be more efficient than oxygen bases of the same pK_a in abstracting a proton from carbon, this greater efficiency is by no means sufficient to account for the observed reactivity differences between tertiary amines and oxygen bases in catalysis of the enolization of oxaloacetic acid. For example, trimethylamine ($pK_a = 10.08$) is about 10 times more reactive than carbonate ($pK_a = 9.77$) in removal of an α-proton from either 2,4-pentanedione or from 3-methyl-2,4-pentanedione and about 35 times more reactive than carbonate in catalysis of nitroethane ionization.[14] However, the present study indicates that trimethylamine is about 1800 times more reactive than carbonate in catalysis of the interconversion of the keto and enol tautomers of oxaloacetic acid. Thus, on the basis of the second-order catalytic rate constants, it is unlikely that tertiary amines catalyze the enolization of oxaloacetic acid by the base catalyzed mechanism (eq 2) established to occur in the presence of oxygen base catalysts, which involves rate-limiting carbanion formation. It would appear that there is a more facile mechanism available for tertiary amine catalyzed enolization.

The intercept values of the tertiary amine buffer dilution plots also suggest that a mechanism other than the well accepted mechanism of eq 2 is followed when the basic catalyst is a tertiary amine. The buffer dilution plots obtained for the reaction of tertiary amines with oxaloacetic acid give well defined intercepts at zero amine concentration (Figure 10). When the logs of the intercepts are plotted on the pH–rate profile vs. the pH at which they were obtained, they fall (solid circles in Figure 11, through which the solid line is drawn) neither on the pH–rate profile established for lyate species catalyzed enolization nor on that established for lyate species catalyzed dehydration. That the rate of the lyate species catalyzed reaction that occurs in the presence of tertiary amines is more than 500-fold greater than can be attributed to keto–enol interconversion and more than 10-fold greater than can be attributed to keto–hydrate interconversion suggests that in the tertiary amine catalyzed enolization reaction

(14) Bruice, P. Y., unpublished data.

lyate species is operating not on keto, enol, or hydrate but on some reactive intermediate.

Because of these unexpectedly high intercept values, the buffer dilution plots of Figure 10 were extended to lower concentrations of tertiary amine, with each solution of tertiary amine containing 0.2 M carbonate buffer to maintain pH. Even at the lowest concentration of tertiary amine employed (8.33×10^{-4} M), the contribution to the observed rate constant from catalysis by amine is greater than the contribution from catalysis by 0.2 M carbonate. The results obtained with 3-quinuclidinol are shown in Figure 13; the other tertiary amines listed in Table III (with the exception of triethylamine) gave similar results. The initial rapid reaction (Figure 13a) is clearly observable down to a tertiary amine concentration of 1.67×10^{-2} M. When the amine concentration is further reduced, the initial reaction is apparent only as a lag phase prior to the subsequent reaction down to a tertiary amine concentration of 8.3×10^{-3} M. When the amine concentration is less than 8.3×10^{-3} M, the initial reaction is not observed at all. The second slower reaction is observed at all concentrations of tertiary amine (Figure 13b); the linearity of the buffer dilution plot, however, is not maintained at low amine concentration. The data of Figure 13b are replotted in Figure 13a so that the magnitude of the two rate processes can be compared. The observation of only a single reaction at low amine concentration indicates that keto–enol interconversion has become slower than keto–hydrate interconversion, and thus only the former reaction is observable. The two buffer plots, therefore, must intersect in order to allow the rate of enolization to become slower than the rate of dehydration. From Figure 13a it is apparent that intersection can occur only if the linearity of the enolization buffer dilution plot is not maintained at low amine concentration. A schematic diagram showing the intersection of the buffer dilution plot for enolization (solid line) and that for dehydration (dashed line) is shown in the inset to Figure 13a. Thus the rate of keto–enol interconversion apparently follows a rate law that is greater than first order in amine at low amine concentration.

The very large second-order rate constants obtained for tertiary amine catalyzed keto–enol interconversion compared to those obtained for catalysis by oxygen bases, the intercepts of the buffer dilution plots that fall neither on the pH–rate profile for enolization nor on that for dehydration, and the failure of the enolization reaction to maintain a first-order dependence on amine at low amine concentration all indicate that the base catalyzed enolization mechanism of eq 2 is not followed when the basic catalyst is a tertiary amine. A mechanism that does account for the above observations is shown in eq 18. This nucleophilic addition–

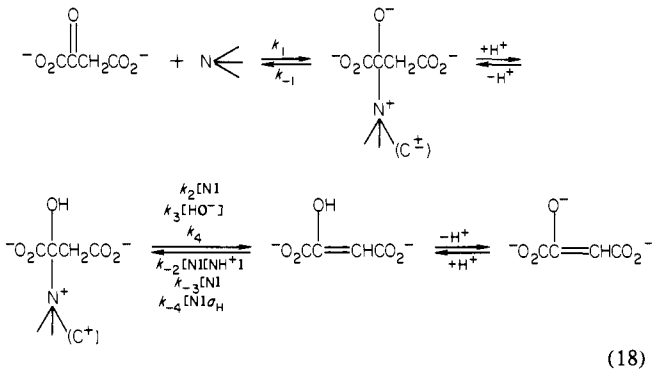

(18)

elimination reaction involves attack of tertiary amine on the ketone carbonyl group to form a zwitterionic carbinolamine ($C^{\pm}$) which is trapped by protonation. A second molecule of tertiary amine reacts with the intermediate carbinolamine (C^{+}) in an E2-type mechanism to give enol by elimination of a proton and neutral amine. Since the rate of collapse of the zwitterionic carbinolamine ($C^{\pm}$) back to starting materials is expected to be more facile than elimination from $C^{\pm}$, the assumption is made that the elimination reaction occurs predominately through C^{+}.

If one assumes steady-state formation of $C^{\pm}$ and C^{+}, the mechanism of eq 18 prescribes the rate expression of eq 19, where

$$k_{obsd} = k_f + k_r = \{k_1k_2a_H[N]^2 + k_1(k_3K_W + k_4a_H) \times [N] + [a_H/(K_E + a_H)]k_{-1}K_{C^+}(k_{-2}a_H[N]/K_N + k_{-3} + k_{-4}a_H)[N]\}/\{k_2a_H[N] + k_{-1}K_{C^+} + k_3K_W + k_4a_H\} \quad (19)$$

K_{C^+}, K_E, and K_N are the acid dissociation constants of C^{+}, enol, and tertiary amine, respectively, and [N] is the concentration of amine present as the free base. Since in the investigated pH range, $a_H > K_E$ and $k_{-3} > k_{-4}a_H$, eq 19 simplifies to

$$k_{obsd} = [a_H(k_1k_2 + k_{-1}k_{-2}K_{C^+}/K_N)[N]^2 + (k_1k_4a_H + k_{-1}k_{-3}K_{C^+} + k_1k_3K_W)[N]]/[k_2a_H[N] + k_{-1}K_{C^+} + k_3K_W + k_4a_H] \quad (20)$$

Assumption of preequilibrium formation of $C^{\pm}$ and C^{+} results in eq 21 where K_1 is the equilibrium constant for formation of

$$k_{obsd} = k_f + k_r = \frac{K_1k_2a_H[N]^2 + K_1(k_3K_W + k_4a_H)[N]}{K_1(K_{C^+} + a_H)[N] + K_{C^+}} + \frac{a_H}{K_E + a_H}(k_{-2}a_H[N]^2/K_N + k_{-3}[N] + k_{-4}a_H[N]) \quad (21)$$

$C^{\pm}$. Since $a_H > K_E$, eq 21 can be rewritten to give

$$k_{obsd} = \{(K_1(K_{C^+} + a_H)k_{-2}a_H/K_N) \times [N]^3 + (K_1k_2a_H + K_1(K_{C^+} + a_H)k_{-3} + K_1(K_{C^+} + a_H)k_{-4}a_H + K_{C^+}k_2a_H/K_N)[N]^2 + (K_1k_3K_W + k_4a_H + K_{C^+}k_{-3} + K_{C^+}k_{-4}a_H)[N]\}/\{K_1(K_{C^+} + a_H)[N] + K_{C^+}\} \quad (22)$$

Assuming that the third-order term in amine in eq 22 can be neglected, both eq 20 and 22 have the mathematical form of eq 23 at any constant pH. At high amine concentration, where

$$k_{obsd} = (K_I[N]^2 + K_{II}[N])/(K_{III}[N] + 1) \quad (23)$$

$K_{III}[N] > 1$, eq 23 predicts the first-order dependence on amine concentration observed in Figure 10. At low amine concentration, the dependence on amine will vary from first to second order depending on the relative values of K_I and K_{II} and the concentration of amine. The exact order in amine is difficult to determine from buffer dilution plots since at low amine concentration there is interference from the hydration equilibrium (Figure 13).

At amine concentrations (>0.02 M) where the first-order dependence on amine concentration is observed, eq 20 for steady-state formation of carbinolamine reduces to eq 24, and eq 22 for

$$k_{obsd} = \left(k_1 + \frac{k_{-1}k_{-2}K_{C^+}}{k_2K_N}\right)[N] + \frac{k_1k_4}{k_2} + \frac{k_1k_3K_W + k_{-1}k_{-3}K_{C^+}}{k_2a_H} \quad (24)$$

$$k_{obsd} = \{(K_1k_2a_H + K_1(K_{C^+} + a_H)k_{-3} + K_1(K_{C^+} + a_H)k_{-4}a_H + K_{C^+}k_2a_H/K_N)[N] + K_1k_3K_W + k_4a_H + K_{C^+}k_{-3} + K_{C^+}k_{-4}a_H\}/K_1(K_{C^+} + a_H) \quad (25)$$

preequilibrium formation of carbinolamine reduces to eq 25. Equation 24 predicts the observed dependence of the intercepts of the linear buffer dilution plots (i.e., those of Figure 10) at zero amine concentration on a spontaneous term and an hydroxide ion dependent term (solid line of Figure 11). If one assumes that $a_H > K_{C^+}$, eq 25 further reduces to eq 26, which also predicts that

$$k_{obsd} = (k_2 + k_{-3} + k_{-4}a_H + K_{C^+}k_2/K_NK_1)[N] + \frac{k_4 + K_{C^+}k_{-4}}{K_1} + \frac{k_3K_W + K_{C^+}k_{-3}/K_1}{a_H} \quad (26)$$

the intercept values will exhibit a spontaneous term and an hydroxide ion dependent term. The pK_a of the hydroxyl group of C^{+} has been estimated to be 11.3 when the amino component of the carbinolamine is protonated methylamine ($pK_a = 10.8$).[5] If one can then assume that the pK_a of the carbinolamine is 0.5 pK_a unit greater than the pK_a of the tertiary amine used to form carbinolamine, then a_H will be sufficiently greater than K_{C^+} for eq 26 to hold for most, but not for all, of the buffer dilution plots determined in this study. Equation 25, however, could also predict the observed pH dependence of the intercept values depending on the magnitude of the individual rate constants. That all of

the intercept values (solid circles) do not fall precisely on the solid line of Figure 11 is not surprising since the solid circles refer to intercepts obtained with a variety of tertiary amines and the constants of the last two terms of eq 24 and 26 are not independent of the amine employed.

Although assumption of either steady-state or preequilibrium formation of carbinolamine in the mechanism of eq 18 fits the observed pH dependence of the intercept values, only the preequilibrium assumption accounts for the ammonium ion dependent catalytic rate constant (k_{1NH}) that is observed with *N,N,N',N'*-tetramethylethylenediamine–H^+. However, the titration curve of Figure 1 argues against an appreciable buildup of carbinolamine in the presence of the tertiary amines listed in Table III. At amine concentrations where the first-order dependence of rate on amine concentration is observed (Figure 10), the preequilibrium assumption requires that $K_1(K_{C^+} + a_H)[N] > K_{C^+}$. For the majority of the buffer dilution plots this can be approximated to $K_1a_H[N] > K_{C^+}$, which can alternately be expressed as in eq 27. Thus at

$$[C^\pm]a_H[N]/([\text{ketone}][N]) > [C^\pm]a_H/[C^+] \qquad (27)$$

amine concentrations greater than ~0.02 M, $[C^+] > [\text{ketone}]$. When ketone is converted to carbinolamine, the keto–enol equilibrium will reestablish decreasing the overall concentration of the enol tautomer. Enol and enolate ion, in particular, are responsible for absorbance of light at 270 nm since neither ketone nor carbinolamine has any appreciable absorbance at that wavelength. Consequently at any given pH, the absorbance at 270 nm of a keto–enol equilibrium mixture in the presence of a tertiary amine should be less than that of the same initial concentration of tautomers in the absence of amine. The circles in Figure 1 indicate the equilibrium absorbance of a 1.13×10^{-4} M solution of oxaloacetic acid in 0.5 M KCl as a function of pH. The triangles in the figure indicate the absorbance of the same concentration of oxaloacetic acid in 0.1 M trimethylamine minus the absorbance of 0.1 M trimethylamine at the given pH. The superimposability of the two plots indicates that there is no appreciable buildup of carbinolamine. It should be pointed out that the data of Figure 1 were difficult to obtain with convincing accuracy. Absorbance readings could not be obtained until establishment of the keto–enol and keto–hydrate equilibria were complete and yet had to be obtained before any significant decarboxylation occurred. The absorbance of the tertiary amine also contributed to the experimental problems involved in looking for small absorbance differences. Several titration plots were determined, and although a few showed loss of absorbance in the presence of tertiary amine, the majority did not.

Under pH decrease conditions, where the substrate is initially equilibrated at pH 12.3 and then mixed with an amine buffer solution at a lower pH, two successive rate processes are observed. Each of these exhibits decreasing absorbance with time (Figure 16). The initial reaction (Figure 16a) shows a significant absorbance change; its rate is linearly dependent on the concentration of protonated amine (Figure 17) and is much faster than any of the amine catalyzed reactions observed in the pH increase experiments. This reaction is most likely attributable to general acid catalyzed protonation of enolate anion by ammonium ion (see Results). The second-order rate constants (k_{3NH}) for the reaction are plotted in Figure 6. Protonated triethylamine and 2-(diisopropylamino)ethanol both exhibit steric hindrance to enolate anion protonation. Steric hindrance to proton transfer from a protonated amine to hydroxide ion or to a general base has been noted previously.[15] The second-order rate constants (k_{3NH}) for protonation of enolate by $HN^+(R)_3$ are about 100-fold greater than those for protonation by HCO_3^- and HPO_4^{2-} (k'_{ga}). This is not surprising considering the electrostatic differences present when the enolate trianion is approached by a positively charged ammonium ion as compared to a general acid containing a negative charge. The Brønsted α values indicate that the extent of protonation in the transition state is greater when the general acid is positively charged (–0.78 vs. –0.59, Figure 6).

The second reaction observed (Figure 16b) in the pH decrease experiments is attributable to the establishment of the keto–enol equilibrium *in* the overall direction of ketone (Table I). The tertiary amine buffer dilution plots obtained for this reaction (Figure 14) exhibit an apparently linear dependence on amine concentration. As was observed in the pH increase experiments, the first-order dependence on amine concentration is not maintained at low concentrations of tertiary amine (Figure 15).

When oxaloacetic acid is mixed with a given buffer solution, the observed rate constant obtained for the enolization reaction should be the same when oxaloacetic acid is originally at pH 12.3 (pH decrease experiment) as it is when oxaloacetic acid is originally equilibrated at pH 2.2 (pH increase experiment). In the presence of tertiary amines, both the pH increase and pH decrease experiments involve overall loss of the enol tautomer. Even if this were not the case, the observed rate constants for the pH increase and decrease reactions are expected to be identical since the enolization reaction involves an approach to an equilibrium position and thus the overall rate constant is given by the sum of the forward and reverse rate constants. In the present study, however, the observed rate constant for keto–enol interconversion is always somewhat greater for the pH increase reaction than it is for the pH decrease reaction; from comparison of rate constants obtained at 0.20 M total amine, the observed rate constant for the former is from 1.3 to 2.9 times greater than that for the latter. The second-order rate constants for the two reactions are close in value (circles in Figure 6), but again those for the pH decrease reaction are consistently smaller. The observed rate differences are probably due to interference from the hydration equilibrium in the determination of the pH decrease rate constants. In the case of the pH increase rates, the decreasing absorbance due to keto–enol interconversion is followed by increasing absorbance due to conversion of hydrate to ketone, and the rates are easily separable. However, in the pH decrease reaction, conversion of enol to ketone and the subsequent conversion of ketone to hydrate are both associated with decreasing absorbance, making it difficult to separate the two rate processes. Experimental observations suggesting that contribution from the hydration equilibrium interferes with accurate determination of observed rate constants for keto–enol interconversion in the pH decrease experiments are as follows: (a) plots of absorbance vs. time are not as clearly first order as are those for the other rate processes in this study; (b) the observed rate constant decreases as the data collection time increases (e.g., the rate constant for keto–enol interconversion catalyzed by 0.1 M 1,4-diazabicyclo[2.2.2]octane is 40.9 and 31.8 s^{-1} with data collection times of 150 and 350 μs/point, respectively); (c) when the buffer dilution plots for tertiary amine catalyzed enolization (Figure 14) are extrapolated to zero amine concentration, some of the intercept values (open circles in Figure 11) fall on the solid line drawn through the enolization intercepts obtained from the pH decrease experiments, but a majority of them fall either precisely on the hydration pH–rate profile or in between the profiles established for hydration and tertiary amine catalyzed enolization. Consequently, the more accurate observed rate constants and second-order rate constants for tertiary amine catalyzed enolization are those obtained from the pH increase experiments.

With the exception of triethylamine and 2-(diisopropylamino)ethanol, the tertiary amines employed in this study have similar steric properties. Triethylamine catalyzes keto–enol interconversion by the nucleophilic addition–elimination mechanism (eq 18) followed by the other, less hindered, tertiary amines; its increased steric bulk is reflected both in the negative deviation of its second-order rate constants from the Brønsted plots of Figure 6 and in the intercept values of the enolization buffer dilution plots (open triangles in Figure 11). However, 2-(diisopropylamino)-ethanol is apparently too bulky to catalyze keto–enol interconversion by the mechanism of eq 18. Its catalytic behavior is

(15) (a) Ralph, E. K., III; Grunwald, E. *J. Am. Chem. Soc.* **1967**, *89*, 2963. (b) Caldin, E. F.; Crooks, J. E. *J. Chem. Soc. B* **1967**, 959. (c) Caldin, E. F.; Crooks, J. E.; O'Donnell, D. *J. Chem. Soc., Faraday Trans.* **1973**, *69*, 1. (d) Bernasconi, C. F. *Acc. Chem. Res.* **1978**, *11*, 147. (e) Bernasconi, C. F.; Carrē, D. J. *J. Am. Chem. Soc.* **1979**, *101*, 2707.

identical with that observed with oxygen base catalysts (see Results). Thus this very sterically hindered tertiary amine catalyzes keto–enol interconversion by the general base catalyzed mechanism of eq 2.

Nucleophilic attack by tertiary amine on the carbonyl group of oxaloacetic acid in the proposed nucleophilic addition–elimination mechanism of eq 18 is certainly not unexpected. Imine and enamine formations which involve nucleophilic attack by primary and secondary amines on carbonyl groups are well accepted mechanisms. Nucleophilic attack by tertiary amine on the enol carbon–carbon double bond, which the proposed mechanism requires in the reverse direction, is not without precedent. Nucleophilic addition of amines to carbon–carbon double bonds activated by electron-withdrawing groups on the α-carbon atom has been extensively studied (eq 28).[15e,16] Bernasconi found that

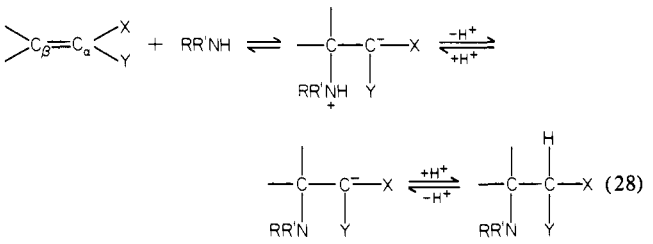

(28)

the kinetic barrier to nucleophilic attack by amine is dependent on the nature of the electrophilic substituent, increasing in the order cyano < ester < nitro. A similar trend has been observed for the kinetic barrier to carbon acid proton transfer.[17] In both cases the kinetic barrier has been related to the degree of electronic organization and concomitant solvational changes with the barrier increasing with increasing charge delocalization.[16e] Nucleophilic addition to olefins containing no activating groups on the α-carbon atom has also been reported. Sprinson has proposed a reversible nucleophilic addition–elimination mechanism for the enzymic synthesis of 5-enolpyruvylshikimate 3-phosphate from phosphoenolpyruvate and shikimate 3-phosphate (eq 29). Cleavage

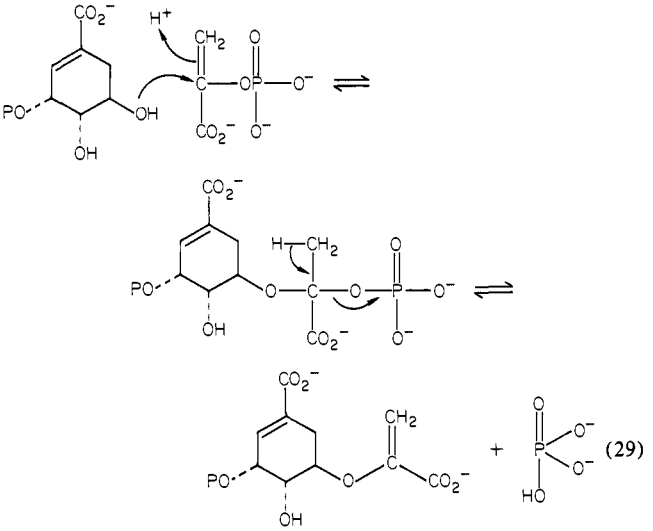

(29)

of the C–OP bond was confirmed by using ^{18}O-labeled phosphoenolpyruvate.[18] A mechanism involving nucleophilic attack on the C-2 carbon of phosphoenolpyruvate has also been proposed for pyruvate uridinediphospho-*N*-acetylglucosamine transferase as well as for tyrosine-sensitive 3-deoxy-D-arabinoheptulosonic acid 7-phosphate synthetase.[19,20] In the case of nucleophilic attack by tertiary amine on enolic oxaloacetic acid, the α-carboxyl group provides some enhancement to nucleophilic attack on the β-carbon atom.

Presumably not all tertiary amine catalyzed keto–enol interconversions will be found to take place by the nucleophilic addition–elimination mechanism of eq 18. Future investigations will be directed toward the elucidation of the structural features that determine the choice between the general base catalyzed mechanism of eq 2 and the nucleophilic addition–elimination mechanism of eq 18.

Although the nucleophilic addition–elimination mechanism has not been previously recognized for keto–enol interconversion, this type of catalysis may find applicability in a variety of organic reaction mechanisms. For example, trimethylamine has been shown to catalyze the aromatization of 4-carbo-*tert*-butoxybenzene oxide via the nucleophilic addition–elimination mechanism of eq 30.[21] Amine catalysis of the dienone-phenol rearrangement has

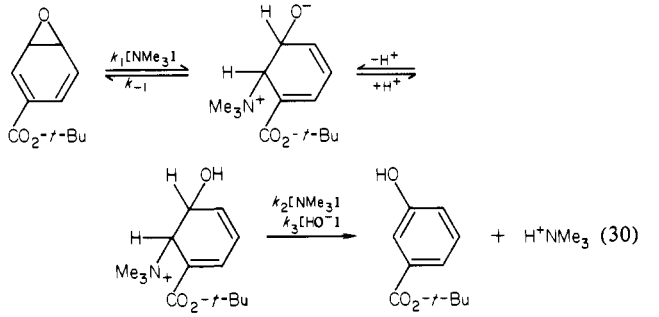

(30)

been attributed to nucleophilic addition of amine followed by rearrangement and elimination of amine.[22] β-Keto and vinylogous β-keto esters are cleaved in ~90% yield by refluxing in *o*-xylene in the presence of a 5-fold excess of 3-quinuclidinol.[23] A possible mechanism involving nucleophilic addition followed by elimination is given in eq 31.

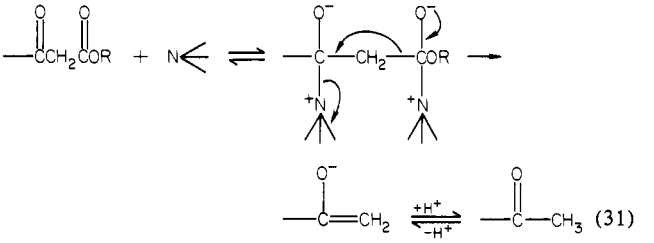

(31)

Emly and Leussing have reported that there is no need to invoke a mechanism other than the general base catalyzed mechanism of eq 2 for tertiary amine catalysis of keto–enol interconversion of oxaloacetic acid since (a) the rate of tertiary amine catalyzed enolization shows a linear dependence on amine at all amine concentrations, (b) the buffer dilution plots for enolization (solid line) and dehydration (dashed line) intersect as shown in the inset to Figure 18, (c) the enolization intercepts fall on the pH–rate profile for general base catalyzed enolization via the mechanism of eq 2, and (d) the high intercepts that we previously reported for enolization could be attributed to our measuring dehydration rates rather than enolization rates above the intersection point, and thus the intercepts should have been assigned to dehydration.[6] In the present study we have shown that (a) the rate of tertiary amine catalyzed enolization shows a linear dependence on amine

(16) (a) Rappoport, Z.; Ladkani, D. *Chem. Sci.* **1974**, *5*, 124. (b) Patai, S.; Rappoport, Z. "The Chemistry of Alkenes"; Patai, S., Ed.; Interscience: New York, 1964; p 469. (c) Bernasconi, C. F.; Carré, D. J. *J. Am. Chem. Soc.* **1979**, *101*, 2698. (d) Schreiber, B.; Martinek, H.; Wolscham, P.; Schuster, P. *J. Am. Chem. Soc.* **1979**, *101*, 4708. (e) Bernasconi, C. F.; Fox, J. P.; Fornarini, S. *Ibid.* **1980**, *102*, 2810. (f) Bernasconi, C. F.; Fornarini, S. *Ibid.* **1980**, *102*, 5329. (g) Bernasconi, C. F.; Carré, D. J.; Fox, J. P. "Techniques and Applications of Fast Reactions in Solution"; Gettins, W. J., Wyn-Jones, E., Eds.; Reidel: Holland, 1979; p 453.

(17) (a) Crooks, J. E. "Proton Transfer Reactions"; Caldin, E., Gold, V., Eds.; Wiley: New York, 1975; p 153. (b) Kresge, A. J. *Acc. Chem. Res.* **1975**, *8*, 354.

(18) Bondinell, W. E.; Vnek, J.; Knowles, P. F.; Sprecher, M.; Sprinson, D. B. *J. Biol. Chem.* **1971**, *246*, 6191.

(19) Zemell, R. I.; Anwar, R. A. *J. Biol. Chem.* **1975**, *250*, 4959.

(20) DeLeo, A. B.; Dazan, J.; Sprinson, D. B. *J. Biol. Chem.* **1973**, *248*, 2344.

(21) Johnson, D. M.; Bruice, T. C. *J. Am. Chem. Soc.* **1975**, *97*, 6901.

(22) Becker, A. R.; Richardson, D. J.; Bruice, T. C. *J. Am. Chem. Soc.* **1977**, *99*, 5058.

(23) Parish, E. J.; Huang, B.; Miles, D. H. *Synth. Commun.* **1975**, *5*, 341.

concentration only at amine concentrations >0.02 M in the pH increase experiments and >0.05 M in the pH decrease experiments (Figures 13 and 15, line c in Figure 18), (b) the buffer dilution plots for enolization (solid line) and dehydration (dashed line) intersect as shown in the inset to Figure 13a, (c) the enolization intercepts are more than 500-fold greater than can be accounted for by the general base catalyzed mechanism of eq 2 (Figure 11), (d) the enolization intercepts are about 10-fold greater than those determined for dehydration, and (e) the second-order rate constants for tertiary amine catalyzed keto–enol interconversion are more than 1000-fold greater than those for catalysis by oxygen bases of the same pK_a, too great a difference to be attributed to the enhanced ability of amines toward proton removal. We have proposed the nucleophilic addition–elimination mechanism of eq 18 to account for these experimental observations.

Registry No. HO^-, 14280-30-9; H_2O, 7732-18-5; PO_4^{3-}, 14265-44-2; HPO_4^{2-}, 14066-19-4; CO_3^{2-}, 3812-32-6; HCO_3^-, 71-52-3; $H_2PO_4^-$, 14066-20-7; oxaloacetic acid, 328-42-7; 2-(diisopropylamino)ethanol, 96-80-0; quinuclidine, 100-76-5; triethylamine, 121-44-8; trimethylamine, 75-50-3; 3-quinuclidinol, 1619-34-7; *N,N,N',N'*-tetramethylethylenediamine, 110-18-9; 1,4-diazabicyclo[2.2.2]octane, 280-57-9; 3-chloroquinuclidine, 42332-45-6; *N,N,N',N'*-tetramethylethylenediamine·H^+, 71889-99-1; *tert*-butyl 7-oxabicyclo[4.1.0]hepta-2,4-diene-3-carboxylate, 57078-21-4.

Directionality of Proton Transfer in Solution. Three Systems of Known Angularity

F. M. Menger,* J. F. Chow, H. Kaiserman, and P. C. Vasquez

Contribution from the Department of Chemistry, Emory University, Atlanta, Georgia 30322.
Received February 2, 1983

Abstract: Three compounds were synthesized each possessing rigid carbon frameworks that hold an oxygen base near a mobile C–H proton in well-defined angular and distance relationships: 2-iodo-4-hydroxyindan, *endo*-5-hydroxybicyclo[2.2.1]heptan-2-one, and *endo*-2-hydroxy-*exo*-6-bromomethyl[2.2.1]heptane. Effective proton transfer was detected with the second and third compounds but not the first. The data suggest that C-to-O proton transfer with severely bent O/H/C angles (106°) is permissible if the O–H distance is less than the sum of the van der Waals radii. "Long distance" catalysis at active sites of enzymes appears unlikely.

"Directionality" refers to the relationship between reactivity and spatial disposition. For example, the directionality of S_N2 substitutions is such that a linear Y/C/X geometry leads to reaction whereas an acute Y/C/X angle does not. Surprisingly, little is known about the directionality of organic reactions in solution. Thus, no information exists on how S_N2 reactivity depends on nucleophile trajectory within the domain of obtuse Y/C/X angles. Information of this kind is required to fully characterize organic pathways and to interpret structural data on enzymes. How can one evaluate a particular arrangement of catalytic groups surrounding a substrate at an active site without first understanding the connection between reactivity and alignment?

Theoretical methods provide one means for dealing with the directionality problem. For example, Stone and Erskine[1] used an intermolecular SCF perturbation theory to examine nucleophilic attack on carbonyl compounds. Energies were calculated as a function of attack angle and approach distance. Despite the considerable merit of such calculations, it must be emphasized (as do Stone and Erskine) that the results pertain only to isolated reactants and that reactants surrounded by solvent could behave quite differently. Nor does the widely quoted solid-state method of Dunitz[2] provide the necessary information. A series of X-ray structures may give an optimum trajectory, but they tell nothing about *other* concurrent trajectories and how they compare with the optimum. Collectively, an array of non-optimal geometries could well dominate a reaction pathway (similar to intermolecular hydrogen bonding where greater than half the population can deviate by 20° or more from the most stable linear structure[3]).

We recently studied the directionality of lactonization reactions with rigid hydroxy acids.[4] Compounds were constructed for which the $HO/C{=}O/C_\alpha$ angles differed by as much as 10° while other factors (such as the HO/C=O distances and ring strain in the lactones) remained constant. It was found that lactonization rates

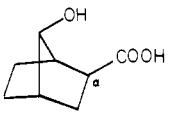

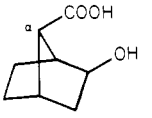

do *not* depend on the angularity differences. Carbonyl additions have, therefore, a "reaction window" of at least 10° (and perhaps much larger). In the present article, we continue the approach of examining reactive functionalities held in space at well-defined angles and distances by rigid carbon frameworks. Three compounds were synthesized each bearing an oxygen in proximity to a mobile C–H proton. The question arises as to whether or not the proton can effectively transfer from carbon to anionic oxygen in the course of an E2 elimination with compounds **1** and **3** or an enolization with compound **2**. The answer to this question

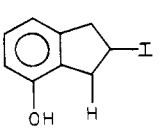

1

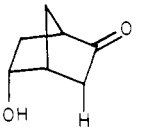

2

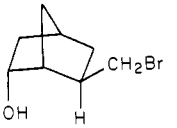

3

was of interest because proton transfer is fundamental to a host of organic and biochemical processes, because the directionality of proton transfer is unknown, and because the $O^-/H/C$ angles in the three compounds are severely bent.

(1) Stone, A. J.; Erskine, R. W. *J. Am. Chem. Soc.* **1980**, *102*, 7185.
(2) Dunitz, J. D. "X-ray Analysis and the Structure of Organic Molecules"; Cornell University Press: Ithaca, N.Y., 1979.
(3) Jorgensen, W. L.; Ibrahim, M. *J. Am. Chem. Soc.* **1980**, *102*, 3309.
(4) Menger, F. M.; Glass, L. E. *J. Am. Chem. Soc.* **1980**, *102*, 5404.

0002-7863/83/1505-4996$01.50/0